

GENERAL INSTRUCTIONS FOR COMPLETING SF 298

The Report Documentation Page (RDP) is used in announcing and cataloging reports. It is important that this information be consistent with the rest of the report, particularly the cover and title page. Instructions for filling in each block of the form follow. It is important to *stay within the lines* to meet *optical scanning requirements*.

Block 1. Agency Use Only (Leave blank).

Block 2. Report Date. Full publication date including day, month, and year, if available (e.g. 1 Jan 88). Must cite at least the year.

Block 3. Type of Report and Dates Covered. State whether report is interim, final, etc. If applicable, enter inclusive report dates (e.g. 10 Jun 87 - 30 Jun 88).

Block 4. Title and Subtitle. A title is taken from the part of the report that provides the most meaningful and complete information. When a report is prepared in more than one volume, repeat the primary title, add volume number, and include subtitle for the specific volume. On classified documents enter the title classification in parentheses.

Block 5. Funding Numbers. To include contract and grant numbers; may include program element number(s), project number(s), task number(s), and work unit number(s). Use the following labels:

C - Contract	PR - Project
G - Grant	TA - Task
PE - Program Element	WU - Work Unit Accession No.

Block 6. Author(s). Name(s) of person(s) responsible for writing the report, performing the research, or credited with the content of the report. If editor or compiler, this should follow the name(s).

Block 7. Performing Organization Name(s) and Address(es). Self-explanatory.

Block 8. Performing Organization Report Number. Enter the unique alphanumeric report number(s) assigned by the organization performing the report.

Block 9. Sponsoring/Monitoring Agency Name(s) and Address(es). Self-explanatory.

Block 10. Sponsoring/Monitoring Agency Report Number. (If known)

Block 11. Supplementary Notes. Enter information not included elsewhere such as: Prepared in cooperation with...; Trans. of...; To be published in.... When a report is revised, include a statement whether the new report supersedes or supplements the older report.

Block 12a. Distribution/Availability Statement.

Denotes public availability or limitations. Cite any availability to the public. Enter additional limitations or special markings in all capitals (e.g. NOFORN, REL, ITAR).

DOD - See DoDD 5230.24, "Distribution Statements on Technical Documents."

DOE - See authorities.

NASA - See Handbook NHB 2200.2.

NTIS - Leave blank.

Block 12b. Distribution Code.

DOD - Leave blank.

DOE - Enter DOE distribution categories from the Standard Distribution for Unclassified Scientific and Technical Reports.

NASA - Leave blank.

NTIS - Leave blank.

Block 13. Abstract. Include a brief (*Maximum 200 words*) factual summary of the most significant information contained in the report.

Block 14. Subject Terms. Keywords or phrases identifying major subjects in the report.

Block 15. Number of Pages. Enter the total number of pages.

Block 16. Price Code. Enter appropriate price code (*NTIS only*).

Blocks 17. - 19. Security Classifications. Self-explanatory. Enter U.S. Security Classification in accordance with U.S. Security Regulations (i.e., UNCLASSIFIED). If form contains classified information, stamp classification on the top and bottom of the page.

Block 20. Limitation of Abstract. This block must be completed to assign a limitation to the abstract. Enter either UL (unlimited) or SAR (same as report). An entry in this block is necessary if the abstract is to be limited. If blank, the abstract is assumed to be unlimited.

THE FLORIDA STATE UNIVERSITY

COLLEGE OF ARTS AND SCIENCES

COMPLEX INDICES OF REFRACTION FOR WATER AND ICE

FROM VISIBLE TO LONG WAVELENGTHS

By

MARK LEE MESENBRINK

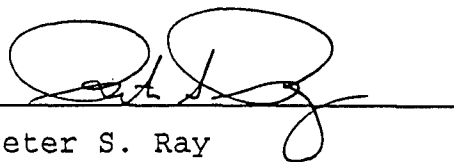
A Thesis submitted to the
Department of Meteorology
in partial fulfillment of the
requirements for the degree of
Masters of Science

Degree Awarded:

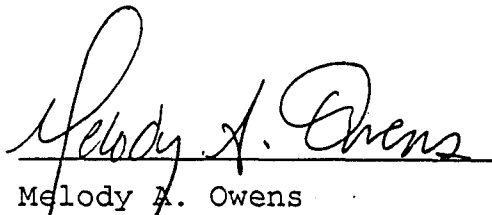
Spring Semester, 1996

The members of the Committee approve the thesis of .

Mark Lee Mesenbrink defended on 28 March, 1996.



Peter S. Ray
Professor Directing Thesis



Melody A. Owens
Committee Member



T. N. Krishnamurti
Committee Member

ACKNOWLEDEMENTS

I would like to acknowledge the many people that have assisted and supported me with my research. My deepest and dearest thanks goes to Cyndi. Without her love, I would not have been able to keep focused. My Committee members, Dr. Peter Ray, Dr. Melody Owens and Dr. T. N. Krishnamurti, deserve many sincere thanks. Without their guidance and instruction, my research would never have been complete. I would like to also thank the three "behind the lines" people who made it all happen: Dr. Craig Bohren from Penn State University for his wisdom; Dr. Jesse Stephens for pointing me in the right directions; and Bret Whissel for his god-like knowledge of FORTRAN and countless other programs. Finally, I would like to thank the Air Force for allowing me the opportunity to further my education.

TABLE OF CONTENTS

	<u>Page</u>
LIST OF TABLES.....	vii
LIST OF FIGURES.....	ix
LIST OF SYMBOLS.....	xii
ABSTRACT.....	xiv
<u>Chapter</u>	
1. INTRODUCTION.....	1
Prologue.....	1
Prior Applications.....	4
Overview of the Data.....	7
Water.....	8
Ice.....	15
2. METHODOLOGY.....	19
Introduction.....	19
Cubic Splines Method.....	20
Debye Regions.....	24
Wörz-Cole Equations.....	27
Weighting.....	28
Summary.....	29
3. RESULTS.....	30

<u>Chapter</u>	<u>Page</u>
Introduction.....	30
Coefficient Equation.....	30
Water.....	31
Visible.....	31
Near Infrared.....	35
Middle Infrared.....	40
Far Infrared.....	46
Microwave/Radiowave.....	50
Longwave.....	52
Summary.....	55
Ice.....	55
Visible.....	55
Near Infrared.....	59
Middle Infrared.....	65
Far Infrared.....	69
Microwave/Radiowave.....	73
Longwave.....	76
Summary.....	76
Uncertainty Incorporation.....	76
4. CONCLUSIONS/FUTURE WORK.....	81
Methodology.....	81
Data.....	82
APPENDICES.....	84
A. DESCRIPTION OF FUNDAMENTALS.....	84

	<u>Page</u>
Vibrational.....	84
Bending.....	85
Rotational.....	85
Hindered Translational.....	86
Orientation.....	86
REFERENCES.....	88
BIOGRAPHICAL SKETCH.....	92

LIST OF TABLES

<u>Table</u>	<u>Page</u>
1.1 List of data sources for water.....	9
1.2 List of data sources for ice.....	10
2.1 Methodology for water.....	29
2.2 Methodology for ice.....	29
3.1 Coefficient data of water in the visible for n.....	32
3.2a Coefficient data of water in the visible for k by Hale and Querry [1973] up to 0.6 μm	36
3.2b Coefficient data of water in the visible for k by Kopelevich [1976] up to 0.6 μm	36
3.2c Coefficient data of water in the visible for k from 0.6 μm to 0.7 μm	36
3.3 Coefficient data of water in the near infrared for n.....	39
3.4 Coefficient data of water in the near infrared for k.....	42
3.5 Coefficient data of water in the middle infrared for n.....	44
3.6 Coefficient data of water in the middle infrared for k.....	46
3.7 Coefficient data of water in the far infrared for n.....	50

<u>Table</u>	<u>Page</u>
3.8 Coefficient data of water in the far infrared for k.....	50
3.9 Coefficient data of ice in the visible for n.	55
3.10 Coefficient data of ice in the visible for k.....	59
3.11 Coefficient data of ice in the near infrared for n.....	59
3.12 Coefficient data of ice in the near infrared for k.....	63
3.13 Coefficient data of ice in the middle infrared for n.....	68
3.14 Coefficient data of ice in the middle infrared for k.....	69
3.15 Coefficient data of ice in the far infrared for n.....	73
3.16 Coefficient data of ice in the far infrared and into the microwave for k.....	75
3.17 Coefficient data of ice in the microwave and into the longwave for k.....	75
3.18 Model uncertainties for water.....	79
3.19 Model uncertainties for ice.....	80

LIST OF FIGURES

<u>Figure</u>	<u>Page</u>
1.1a Sources used by Ray [1972] for water.....	2
1.1b Sources used in this study for water.....	2
1.2a Sources used by Ray [1972] for ice.....	3
1.2b Sources used in this study for ice.....	3
3.1 Real part of the complex index of refraction for water in the visible region.....	33
3.2 Imaginary part of the complex index of refraction for water in the visible region.....	34
3.3 Real part of the complex index of refraction for water in the near infrared region..	38
3.4 Imaginary part of the complex index of refraction for water in the near infrared region.....	41
3.5 Real part of the complex index of refraction for water in the middle infrared region.....	43
3.6 Imaginary part of the complex index of refraction for water in the middle infrared region.....	45
3.7 Real part of the complex index of refraction for water in the far infrared region.....	48
3.8 Imaginary part of the complex index of refraction for water in the far infrared region...	49
3.9 Complex indices of refraction for water in the microwave/radiowave region.....	53

<u>Figure</u>	<u>Page</u>
3.10 Complex indices of refraction for water in the longwave region.....	54
3.11 Complex indices of refraction for water over entire spectrum in this study.....	56
3.12 Real part of the complex index of refraction for ice in the visible region.....	57
3.13 Imaginary part of the complex index of refraction for ice in the visible region.....	58
3.14 Real part of the complex index of refraction for ice in the near infrared region.....	60
3.15 Imaginary part of the complex index of refraction for ice in the near infrared region....	64
3.16 Real part of the complex index of refraction for ice in the middle infrared region.....	66
3.17 Imaginary part of the complex index of refraction for ice in the middle infrared region..	67
3.18 Real part of the complex index of refraction for ice in the far infrared region.....	71
3.19 Imaginary part of the complex index of refraction for ice in the far infrared region.....	72
3.20 Complex indices of refraction for ice in the microwave/ radiowave region.....	74
3.21 Complex indices of refraction for ice in the longwave region.....	77
3.22 Complex indices of refraction for ice over entire spectrum in this study.....	78
A.1 Symmetrical stretching, ν_1 , (left) and asymmetrical stretching, ν_3 , (right).....	84
A.2 Bending fundamental, ν_2	85
A.3 Rotational, or Librational, fundamental, ν_L ..	86

<u>Figure</u>	<u>Page</u>
A.4 Hindered Translational fundamental, v_T	87

LIST OF SYMBOLS

α	Lambert absorption coefficient
atm	atmosphere, pressure unit
b_1, b_j	breakpoints
c	speed of light (3.0×10^8 meters per second)
$C_1, C_2 \dots$	coefficients
cm	centimeter
$^{\circ}\text{C}$	degrees Celsius
dc	direct current
δ	loss angle
EHF	Extremely High Frequency
E-M	electromagnetic
ϵ	complex permittivity
ϵ'	real part, dielectric constant
ϵ''	imaginary part, dielectric loss
ϵ_{∞}	high frequency dielectric constant
ϵ_0, ϵ_s	static dielectric constant
f	frequency
f	function
GHz	Giga Hertz (10^9 cycles per second)
h	breakpoint separation
H	hydrogen atom
I _h	Phase I ice in hexagonal lattice
ir	infrared
k	imaginary part of m
K	degrees Kelvin
LWC	Liquid Water Content
λ	wavelength
λ_s	relaxation wavelength
m	meter
m	complex index of refraction
mm	millimeter
μm	micrometer (10^{-6} meter)
n	real part of m
nm	nanometer (10^{-9} meter)
ν	wavenumber
ν_1, ν_2, ν_3	molecular fundamentals

O	oxygen molecule
π	constant = 3.141.....
R	reflectance
RMS	Root Mean Square
σ	conductivity
u_p	phase velocity
uv, UV	ultraviolet

ABSTRACT

The purpose of this study is to develop empirical relationships that model the complex refractive index of water and ice from visual to long wavelengths. Prior applications employing modeled complex indices of refraction for water and ice are presented.

Complex index of refraction data is compiled from researchers who have taken measurements of reflectance and absorption in various spectral regions, and derived the real and imaginary parts, n and k , from these quantities. The spectral domain under investigation is divided into six sub-regions. These regions are: visible, near infrared, middle infrared, far infrared, microwave/radiowave, and longwave. The corresponding wavelength increments are: 0.4 micrometers to 0.7 micrometers, 0.7 micrometers to 4 micrometers, 4 micrometers to 50 micrometers, 50 micrometers to 1 millimeter, 1 millimeter to 100 meters and greater than 100 meters. The data are modeled as a function of wavelength and temperature. The temperature range modeled is representative of the troposphere. Water is investigated between 30 degrees Celsius and -10 degrees Celsius. Ice is

investigated between 0 degrees Celsius and -80 degrees Celsius. Model results from each wavelength interval are discussed individually to outline significant features. Possible needs for future research are presented.

CHAPTER 1
INTRODUCTION

Prologue

Modeling the complex indices of refraction for water and ice is necessary for several areas of Meteorology, especially remote sensing. This study is an extension of Ray [1972], where the complex indices of refraction of water and ice were modeled through empirical formulae. The present investigation will extend from the visible spectrum to wavelengths greater than one kilometer, using data that has become available after Ray's study. Some sources of refractive index data used in this study compiled values also used by Ray.

Figures 1.1a, 1.1b, 2.1a and 2.2b show the coverage of data used by Ray [1972] and for the present study. As shown by the figures, more measurements are available, particularly for ice. The increased accuracy and amount of refractive index data will improve the empirical model of the refractive indices for ice.

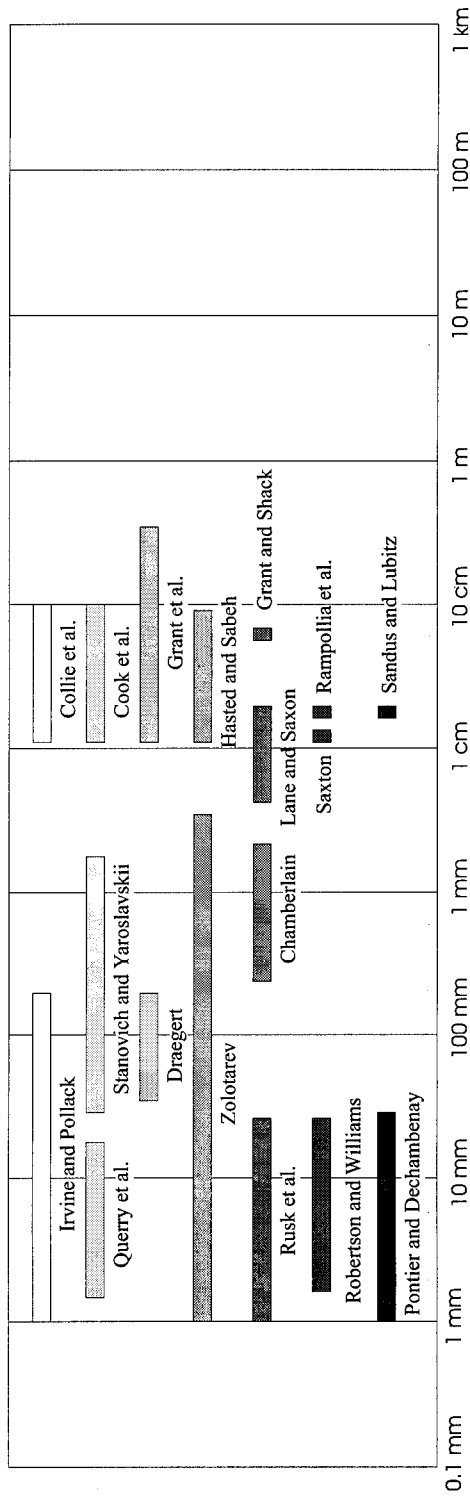


Figure 1.1a. Sources used by Ray [1972] for water.

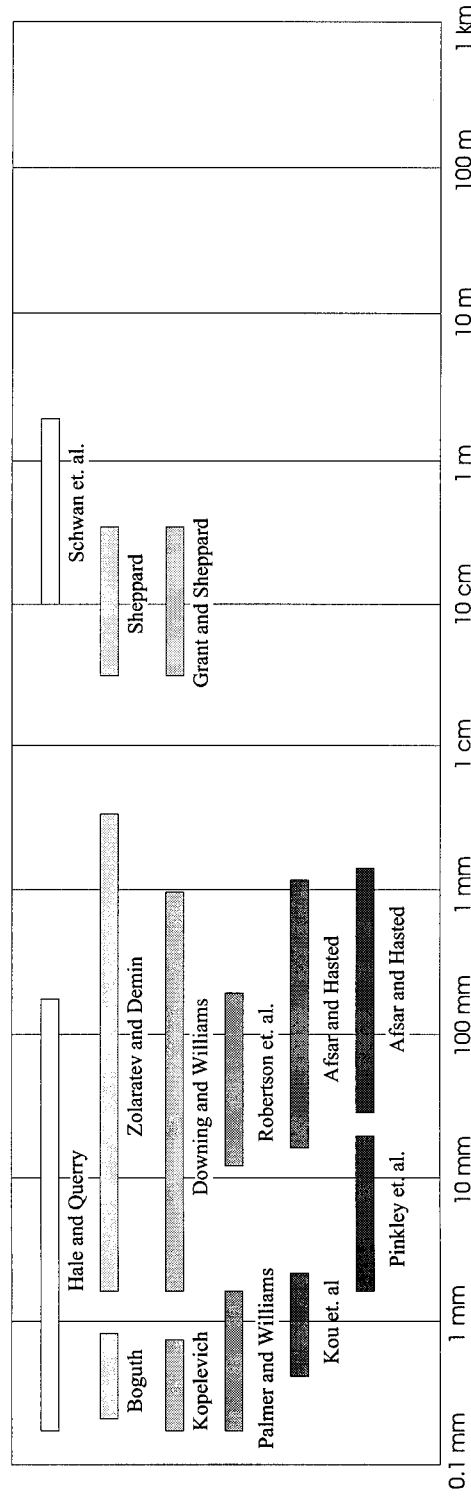


Figure 1.1b. Sources used in this study for water.

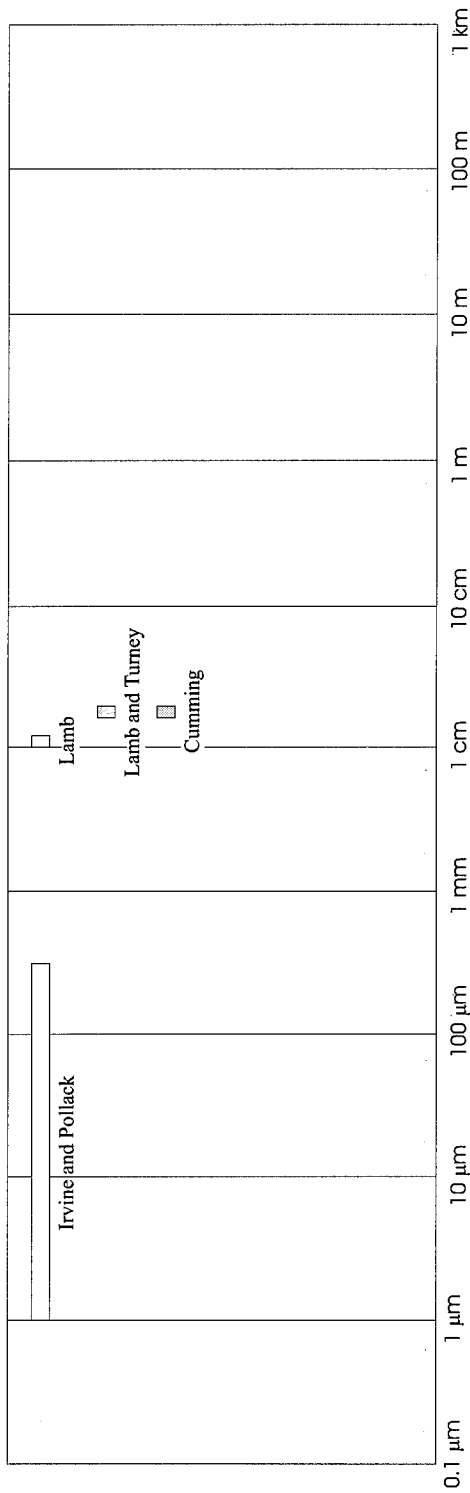


Figure 1.2a. Sources used by Ray [1972] for ice.

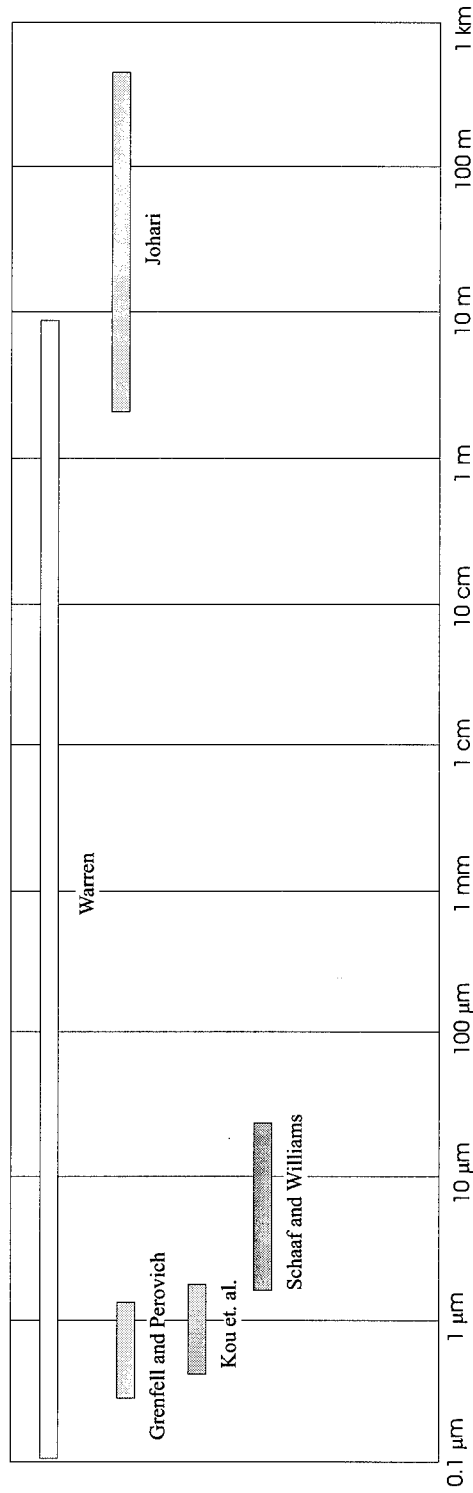


Figure 1.2b. Sources used in this study for ice.

The form of the complex index of refraction used in this study is given by the equation

$$m(\lambda) = n(\lambda) - ik(\lambda), \quad 1.1$$

where the real part, n , determines the phase velocity, and the imaginary part, k , determines attenuation. References to the "real part" and the "imaginary part" in this study will refer to n and k , respectively, unless specified otherwise. Some of the data used are complex dielectric constants. The conversion of these data to the complex index of refraction expressions is discussed later in this chapter.

Prior Applications

The results from Ray's paper have been applied to many research problems. The primary application is that of modeling radiation transfer. Many models of electromagnetic energy propagating in media impregnated with water or ice have used the results from Ray's work. A few specific applications of modeled equations for the complex indices of water and ice are presented below.

Liu and Curry [1992] developed an algorithm to retrieve precipitation from Special Sensor Microwave/Imager (SSM/I) satellite data. These satellites operate in the microwave region of the electromagnetic spectrum at frequencies of 19.35, 22.235, 37 and 85.5 GHz. To determine precipitation

from the data, the microwave radiative transfer equation was solved using emission and scattering coefficients for water and ice particles. Ray's empirical equations were used to solve for these quantities at the given frequencies.

Shimabukuro et al. [1984] derived extremely high frequency (EHF) attenuation from emission temperatures in light rain using the radiometric formula. For the range of frequencies considered in this study, water and ice are absorptive. The authors used the attenuation expression:

$$\alpha_c = 8.186 \frac{LWC}{\lambda} \operatorname{Im} \left(-\frac{m^2 - 1}{m^2 + 2} \right) \quad \text{dB} \cdot \text{km}^{-1}. \quad 1.2$$

In this expression, the quantity of interest is complex index of refraction, m , which is calculated using the formulae from Ray's study.

Jameson [1990] evaluated several microwave parameters to rainfall rate in order to identify an accurate measurement of rain. Some of the parameters investigated were polarization, phase change rates, backscatter and attenuation rates. The relation of these parameters to drop size enables an estimate of rainfall rate. The purpose of this research is to determine the best real-time method of estimating rain rates. Jameson computed complex indices of refraction values using the relations from Ray in the compilation of backscatter calculations.

Jameson [1992] investigated the effects of temperature dependence on attenuation. The calculated attenuation is used to improve radar reflectivity estimates. The types of radar being evaluated are those using dual polarization operating at frequencies between 10 and 3 GHz. Jameson uses Ray's empirical formulae to obtain values for water at different temperatures. From his evaluation, Jameson found temperature dependence should be included in radiometric modeling involving electromagnetic propagation at frequencies below 10 GHz.

Adler et al. [1991] uses a coupled cloud physics-radiative transfer model to replace the more simplified layered structures used by other authors studying rainfall estimates from space observation platforms. The benefit is a more realistic model to produce radiative transfer model values closer to the actual ones. The same microwave radiative transfer model used by Liu and Curry [1992] is also used by these authors. The formulae presented by Ray are used to compute the real and complex parts of the indices of refraction needed to solve this form of the radiative transfer equation.

As can be seen from these applications, this work is very useful in radiative transfer models and attenuation correction calculations. Rain rate estimation and correction calculations also have a need for this work.

Overview of the Data

The data used for this study are from 17 authors in 25 studies. Each study covered small to intermediate portions of the E-M spectrum. Some are region specific, i.e. visible or infrared; however, some author's refractive index data span many regions, such as Zolaratev and Demin [1977], who investigate a broadband region from ultraviolet to microwave. Having many data sets from many authors posed another problem, that of the data having been measured for a wide range of temperatures. To simplify the choice of data, only those data sets measured at temperatures of meteorological significance were chosen. Water temperature ranges accepted were -30°C to $+30^{\circ}\text{C}$. Ice temperature ranges accepted were -70°C to 0°C . Though these criteria were used to exclude extreme temperatures, not all temperatures in these ranges were represented with the data collected.

Many investigators made optical constant measurements on different phases of ice. The one phase prevalent to meteorology is the phase I_h , where h denotes a hexagonal lattice structure. This is the only naturally occurring phase of ice with the atmospheric conditions present on Earth. Other phases can be reached by applying intense pressure which may be reached deep within ice packs. To present an example of how much pressure is needed to change

phases, it would take a pressure of approximately 2 kilobars at -40°C to go from phase Ih to phase II. This is equivalent to slightly less than 2000 times standard surface pressure.

Some data sets were measured under pressures in excess of 100 bars. Again, only meteorological significant pressures are considered in this study. All data used will be under standard surface atmospheric pressure of 1 bar or, 1 atm. To illustrate the effects of pressure, Srinivasan and Kay [1974] made high pressure measurements of the dielectric constant for water. The dielectric constant at 500 bars declined 8.8 percent from the value at 1 bar. Pressure within the troposphere does not vary this highly, and should not be a factor to be considered.

Data from both phases of water will be discussed. Parameters of measurement, method of measurement, and uncertainty estimation will be covered. A complete chart of data used are in Table 1.1 for water and Table 1.2 for ice.

Water

Hale and Querry [1973] compiled Lambert absorption coefficients, reflectance and k values from several investigators made in a wide spectral region. They took their analysis into from the x-ray to the far infrared regions corresponding to wavelengths of 200 nm to 200 μm .

The imaginary values, $k(\lambda)$, were determined and a subtractive Kramers-Kronig analysis was made to find $n(\lambda)$,

Table 1.1. List of data sources for water.

Author(s)	Wavelengths	Temperature	Uncertainty
Hale and Querry	200 nm - 200 μ m	25°C	Varies
Boguth	250 nm - 700 nm	23°C	< 5%
Kopelevich	250 nm - 600 nm	20°C	Varies
Kou, et al.	0.65 μ m - 2.5 μ m	22°C, -8°C	< 10%
Palmer and Williams	0.36 μ m - 2.6 μ m	27°C	2%
Zolaratev and Demin	0.1 Å - 1 m	25°C	3-5%
Downing and Williams	2 μ m - 1 mm	27°C	4%
Pinkley, et al.	2 μ m - 25 μ m	1°C, 16°C	< 1%
Robertson, et al.	12.5 μ m - 200 μ m	unknown	< 5%
Afsar and Hasted	45.5 μ m - 2 mm	4°C, 30°C	< 5%
Afsar and Hasted	22.2 μ m - 1.7 mm	19°C	< 5%
Sheppard	7.46 cm - .645 m	4°C	< 5%
Grant and Sheppard	7.46 cm - .645 m	4°C	< 5%
Sheppard and Grant	10 cm - 3 m	25°C	< 3%

Table 1.2. List of data sources for ice.

Author(s)	Wavelengths	Temperature	Uncertainty
Kou, et al.	0.65 μm - 1.45 μm	-25°C	< 10%
Schaaf and Williams	2 μm - 33.3 μm	-7°C	< 4%
Grenfall and Perovich	0.4 μm - 1.4 μm	-4°C	< 20%
Warren	44 nm - 8.6 m	-7°C, Varies	Varies
Johari	3 m - 600 m	-5°C	< 2%
Johari and Charette	5 m, 8.6m	Varies	< 2%

given by

$$n(\lambda_0) = 1 + \frac{2\lambda_0^2}{\pi} \text{P} \int_0^\infty \frac{k(\lambda)d\lambda}{\lambda(\lambda_0^2 - \lambda^2)}. \quad 1.3$$

The integrand is taken from long to small wavelengths, λ , for each wavelength of interest, λ_0 . The P signifies the Cauchy principle value needed to integrate around the pole when λ_0 is equal to λ . A form of the Cauchy principle value is given by

$$\lim_{a \rightarrow 0} \int_0^{\omega-a} \frac{\chi(\Omega)}{\Omega - \omega} d\Omega + \lim_{a \rightarrow 0} \int_{\omega+a}^\infty \frac{\chi(\Omega)}{\Omega - \omega} d\Omega. \quad 1.4$$

The temperature chosen was approximately 25°C. Since values were compiled from many authors, the uncertainty of these values is variable. Hale and Querry do not list the

individual uncertainties of each author or do not give uncertainties of their calculated values of n .

Boguth [1973] measured values of n from the uv region to the visible corresponding to wavelengths of 254 nm to 707 nm. The measurements were carried out using a spectrometer and four different spectral lamps as sources. The uncertainty of the measurements is $\pm 0.0015\%$. These measurements were taken at a temperature of 23°C .

Kopelevich [1976] investigated from the UV region to the visible. Kopelevich, like Hale and Query [1973], compiled existing Lambert absorption coefficients and k measurements from other authors. Kopelevich criticized the ceresin lining of the measurement cell associated with the data used by Hale and Query [1973] in the visible region. The data compiled by Kopelevich used a silver lining. According to Kopelevich, this lining gives more reliable results. These criticisms will be taken into consideration when the data are fit. The temperature at which these values were taken was 20°C . Kopelevich, like Hale and Query, did not report any statistical uncertainties of the data used.

The measurements of absorption coefficients made by Kou et al. [1993] ranged from the edge of the visible region into the near infrared. From the absorption coefficients, k

was calculated and tabulated. Their measurements were for supercooled water, -8°C , and water at room temperature, 22°C . They also took measurements for ice at -25°C . The measurements were obtained using a Bomem DA3.02 Fourier-Transform infrared spectrometer. The authors estimate uncertainties less than 10%.

Palmer and Williams [1974] made measurements in the visible and near infrared bands at wavenumbers 3800 to 27800 cm^{-1} , corresponding to wavelengths of $2.6\text{ }\mu\text{m}$ to roughly $0.36\text{ }\mu\text{m}$. The Lambert absorption coefficient, $\alpha(\nu)$, and reflectance, R , was obtained from a double-pass prism monochromator. From the Lambert absorption coefficient, the imaginary part of the complex index of refraction was obtained from the equation

$$k(\nu) = \frac{\lambda\alpha(\nu)}{4\pi}. \quad 1.5$$

The real part was obtained by using the Fresnel expression for normal-incidence spectral reflectance

$$R = \frac{(n-1)^2 + k^2}{(n+1)^2 + k^2}. \quad 1.6$$

The authors use the approximation that k is very small and can, therefore, be neglected. This approximation is valid because the largest magnitude of k^2 is of order 10^{-5} as compared to the corresponding value of $(n-1)^2$, of order

10^{-2} . The approximation resulted in the equation

$$n = \frac{1 + \sqrt{R}}{1 - \sqrt{R}}. \quad 1.7$$

These measurements were made at 27°C with uncertainties less than 2%.

Zolaratev and Demin [1977] made reflectance measurements through the near and middle infrared regions, corresponding to wavelengths of 2 μm to 50 μm . With the use of k values from other authors, this interval was extended from 0.1 \AA to 1 m. From these measurements and supplemental data, the Fresnel and Kramers-Kronig relations was used to calculate n and k, as was done by Palmer and Williams [1974]. Data for n and k tabulated by Zolaratev and Demin are given for wavelengths of 2 μm to 5 cm, which corresponds to the near infrared to the microwave/radiowave portions of the spectrum. The method used to obtain reflectance measurements of the near and middle infrared data involved a double-beam infrared spectrophotometer. Zolaratev and Demin declare uncertainties in the measurements and in the calculations between 3-5%. The measurements were made at 20°C.

Nearly the entire infrared broadband was investigated by Downing and Williams [1975]. Their study covers wavelengths from 2 μm to 1000 μm . This work consists of a

compilation of Lambert absorption coefficient measurements obtained by other authors. From these values, the Kramers-Kronig relation

$$n(\nu) = 1 + (2\pi^2)^{-1} \text{P} \int_0^{\infty} \frac{\alpha(\nu') - \alpha(\nu)}{\nu'^2 - \nu^2} d\nu' \quad 1.8$$

was used to calculate the real part, n . The values of k were calculated directly from the absorption coefficients. Downing and Williams declare uncertainties of $\pm 1\%$ and $\pm 4\%$ for n and k , respectively. These measurements were taken at 27°C .

The influence of temperature on water in the near to middle infrared bands, corresponding to wavelengths of $2 \mu\text{m}$ to $25 \mu\text{m}$, is studied by Pinkely et al. [1976]. Absorption, reflectance and k data were compiled at four different temperature measurements, 1°C , 16°C , 39°C , and 50°C . The values for n were calculated using the Fresnel and Kramers-Kronig relations, as was done by Palmer and Williams [1974]. Only the first two temperatures are utilized in this study. The n and k values tabulated by Pinkley et al. have uncertainties of $\pm 1\%$ and $\pm 3\%$, respectively.

Afsar and Hasted [1976, 1978] conducted two separate measurements of the Lambert absorption coefficients using a reflection-dispersive-Fourier-transform-spectrometric

technique, within roughly the same broadband. The 1976 study was made at wavelengths of 22.2 μm to 1.7 mm. The uncertainties of n and k are $\pm 0.5\%$ and $\pm 5\%$, respectively. The temperature for this experiment was 19°C . In the 1978 study, measurements of α were made between 45.5 μm to 2 mm. Afsar and Hasted made these measurements at three different temperatures: 4°C , 30°C and 57°C . Only the first two temperatures were used in the current study. The uncertainties n and k were the same as those reported in the 1976 study.

Ice

Absorption measurements of ice were made by Kou et al. [1993] in the near infrared region. The methodology of retrieving these measurements, as well as statistical information were discussed in the water section of this chapter. Measurements were made at -25°C .

A reflectometer and spectrometer were used to make measurements of reflectance in the near to middle infrared by Schaaf and Williams [1973]. The wavelengths corresponding to their experiment were 2 μm to 33.3 μm . The authors used expressions relating n and k to reflectance, R :

$$n = \frac{1-R}{1+R-2\sqrt{R\cos\phi}} \quad 1.9$$

$$k = \frac{-2\sqrt{R \sin \phi}}{1 + R - 2\sqrt{R \cos \phi}}, \quad 1.10$$

where ϕ was calculated using the Kramers-Kronig phase integral

$$\phi(\nu_0) = (2\nu_0/\pi) \mathcal{P} \int_0^{\infty} \frac{\ln \sqrt{R(\nu)}}{\nu^2 - \nu_0^2} d\nu. \quad 1.11$$

Measurements were made at -7°C . The uncertainties of n and k are $\pm 2\%$ and $\pm 4\%$, respectively.

Warren [1984] compiled optical constant data from several authors. The optical constant data, absorption coefficient, permittivity, reflectance and k , were used to make a tabulation of k . From the k data, n was calculated using the Kramers-Kronig equation. The spectral interval was 44 nm to 8.6 m. The temperatures of Warren's study vary. From 44 nm to 167 μm , the temperature is -7°C . Four different temperatures were presented in the interval of 167 μm to 8.6 m. These temperatures are -1°C , -5°C , -20°C and -60°C . Ice exhibits the greatest temperature dependence within this region. This temperature dependence will be discussed in further detail in Chapter 3. The uncertainties vary in Warren's study. Statistical information was given by Warren for some of the data used.

The absorption coefficients, α , were measured by Grenfell and Perovich [1981] in the visible and near infrared regions. The wavelengths corresponding to this interval are .4 μm to 1.4 μm . A collimated beam of light was projected through a block of bubble-free ice, and intensity measurements were made by a scanning photometer, from which the absorption coefficient was calculated. The maximum uncertainty was $\pm 20\%$ in the range of 0.4 μm to 0.42 μm . The remainder of the interval has uncertainties approximately $\pm 10\%$. These uncertainties are very acceptable in this region for the complex part. This is because k is on the order of 10^{-9} at 0.4 μm and increases to 10^{-5} at the end of the interval of 1.4 μm . The absorption coefficients measured range from nearly 10^{-3} to 10^{+2} . Six orders of magnitude show high variability in this small spectral region. The measurements were taken at -4°C .

Longwave measurements were made by Johari [1976] for wavelengths of 3 m to 600 m. A Hewlett-Packard model 4271A LCR meter was used to obtain electromagnetic properties such as permittivity, ϵ' , and dissipation factor, $\tan\delta$. The loss factor, ϵ'' , may have been measured or calculated using

$$\tan\delta = \frac{\epsilon''}{\epsilon'}. \quad 1.12$$

The real and imaginary parts of the index of refraction were calculated using the relations

$$\epsilon'' = 2nk \quad 1.13$$

$$\epsilon' = n^2 - k^2. \quad 1.14$$

The permittivity and loss factor measurements had uncertainties of $\pm 0.3\%$ and $\pm 2\%$, respectively. Since both ϵ' and ϵ'' were used to calculate n , and k , $\pm 2.02\%$ should be used as a combination of the two uncertainties. This uncertainty is valid for both n and k . The equations used to calculate n and k from ϵ' and ϵ'' are as follows:

$$n = \left(\frac{((\epsilon'^2 + \epsilon''^2)^{\frac{1}{2}} + \epsilon')}{2} \right)^{\frac{1}{2}} \quad 1.15$$

$$k = \left(\frac{((\epsilon'^2 + \epsilon''^2)^{\frac{1}{2}} - \epsilon')}{2} \right)^{\frac{1}{2}}. \quad 1.16$$

These measurements were made at -5°C .

Johari and Charette [1975] made measurements of relative permittivity, ϵ' and dielectric loss, $\tan\delta$, of ice at two wavelengths, 5 m and 8.6 m. Temperature was varied between -1.0°C to -25.0°C for both wavelengths. The methodology used was the same as that in the previously discussed work. As such, the uncertainty is also the same.

CHAPTER 2
METHODOLOGY

Introduction

The purpose of this study is to create empirical formulae that model the real and complex refractive indices of ice and liquid water over a wide frequency range.

Many curve fitting methods were considered. Because of the complexity of the curves to be fit, a high order polynomial may seem like the best solution; however, with the many maxima and minima, a high order polynomial will extend and exaggerate the observed maximum and minimum values.

The spectral domain under investigation is divided into six sub-regions. These regions are: visible, near infrared, middle infrared, far infrared, microwave/radiowave, and longwave. The corresponding wavelength increments are: 0.4 micrometers to 0.7 micrometers, 0.7 micrometers to 4 micrometers, 4 micrometers to 50 micrometers, 50 micrometers to 1 millimeter, 1 millimeter to 100 micrometers and greater than 100 micrometers. These

spectral bands will be further segmented using knots and cubic splines fit to these sections. The resulting cubic equations can easily be programmed into any application or model requiring the complex index of refraction for water or ice in the needed spectral regions.

The mathematical relationship between n and k is described by the Kramers-Kronig relations. These relations ensure the behavior between n and k is maintained. In addition, the Kramers-Kronig relations present a tool for calculating n from k or visa versa. To derive one optical constant from another using the Kramers-Kronig relation, one quantity must be measured in a broadband spectrum. Since the scope of this study is to produce empirical formulae modeling n and k , the utilization of the Kramers-Kronig relation is not feasible. Much of the data used has been calculated using the Kramers-Kronig relation, satisfying the spectral dependence.

Cubic Splines Method

Cubic splines present a technique where the coefficients can be "forced" to pass through several points. The spline program used reduces a region into evenly spaced breakpoints. The data between these breakpoints are used to derive the coefficients of a third-order polynomial. Having a low order polynomial fit reduces the fluctuations found in

high order polynomial interpolation schemes. Each breakpoint can be thought of as a knot connecting each cubic segment. The breakpoints of each segment have been adjusted to give the smallest residual. Since all of the spectral regions have different behaviors, the number of breakpoints will differ. The fewer breakpoints used will produce fewer cubic polynomials and visa versa. If needed, more breakpoints will be added to reduce the residuals.

The cubic spline fitting method implemented in this study comes from Lawson and Hanson [1974]. The data interval is broken up into evenly space breakpoints or knots so that

$$b_1 < b_2 < \dots < b_n \quad , \quad 2.1$$

where b_1 and b_n are the endpoints of the data segment and $b_2 \dots b_{n-1}$ are the internal knots. The distance between each breakpoint is defined as

$$h = b_{k+1} - b_k \quad (k = 1, \dots, n-1). \quad 2.2$$

The family of independent splines in the interval $[b_1, b_n]$ can be denoted as S , where f is an individual cubic equation on each interval $[b_k, b_{k+1}]$. The function, f , takes on the form

$$f(x) = \sum_j c_j q_j(x) . \quad 2.3$$

The limit, j , constitutes $n+2$ independent functions within the vector space, S . If the set of data, (x_i, y_i) , is

contained within the breakpoint interval, $[b_1, b_n]$, the solution of individual equations making up S becomes a matrix problem of the form

$$Ac \cong y, \quad 2.4$$

where the elements of matrix A are

$$a_{ij} = q_j(x_i) \quad i = 1, \dots, m \quad 2.5$$

$$j = 1, \dots, n+2,$$

so that A is an m by n+2 matrix. Each individual piece of matrix A, a_{ij} , represents a function, $q_j(x_j)$. Since the function is a third order polynomial of the form

$$a_0 + a_1x + a_2x^2 + a_3x^3, \quad 2.6$$

and the ordinate data is organized such that

$$x_1 \leq x_2 \leq \dots \leq x_m, \quad 2.7$$

the band width, or number of non-zero terms in a matrix row of A, will be four.

Lawson and Hanson define two cubic polynomials

$$p_1(t) = 0.25t^3 \quad 2.8$$

and

$$p_2(t) = 1 - 0.75(1+t)(1-t^2), \quad 2.9$$

where

$$t = \frac{x - b_k}{h}. \quad 2.10$$

Within each breakpoint interval, four functions, q_{ij} , have non-zero values:

$$q_k(x) = p_1(1-t) \quad 2.11$$

$$q_{k+1}(x) = p_2(1-t) \quad 2.12$$

$$q_{k+2}(x) = p_2(t) \quad 2.13$$

$$q_{k+3}(x) = p_1(t) . \quad 2.14$$

The breakpoints in the algorithm are coded using the formula

$$b_i = x_1 + \frac{x_m(i-1)}{NBP-1} \quad (i = 1, \dots, NBP), \quad 2.15$$

where NBP is the number of breakpoints to be used. Notice that the minimum number of breakpoints is 2, which corresponds to the endpoints of the data set.

The root-mean square is calculated to determine the error between the data set and the fitted curves, using

$$RMS = \left(\frac{\sum_{i=1}^m r_i^2}{m} \right)^{\frac{1}{2}}, \quad 2.16$$

where r_i represents the residuals between the data and the fit, and m is the data set length.

The coefficients of the polynomial given by equation 2.6 are found by adding equations 2.11 through 2.14. The coefficients were found to be

$$a_0 = \frac{1}{4}C_1 + C_2 + \frac{1}{4}C_3 \quad 2.17$$

$$a_1 = -\frac{3}{4}C_1 + \frac{3}{4}C_3 \quad 2.18$$

$$a_2 = \frac{3}{4}C_1 - \frac{6}{4}C_2 + \frac{3}{4}C_3 \quad 2.19$$

$$a_3 = -\frac{1}{4}C_1 + \frac{3}{4}C_2 - \frac{3}{4}C_3 + \frac{1}{4}C_4, \quad 2.20$$

where C_1 through C_4 are from the coefficient matrix computed by the FORTRAN algorithm. The coefficients presented in Chapter 3 are the empirical coefficients that represent the behavior of the data.

Some additions were made to the program from Lawson and Hanson. A high resolution computation was coded to give a smoother representation of the fitting. The program had to be altered to accommodate loading data from ASCII files.

Debye Regions

Water and ice (Ih) both have regions of significant temperature dependence. From Debye [1929], it is customary to use the complex permittivity. From Debye's theory, the dielectric constants can be expressed by the following relations:

$$\epsilon' = \epsilon_\infty + \frac{\epsilon_0 - \epsilon_\infty}{1 + \left(\frac{\lambda_s}{\lambda}\right)^2} \quad 2.21$$

$$\epsilon'' = \frac{(\epsilon_0 - \epsilon_\infty) \left(\frac{\lambda_s}{\lambda}\right)}{1 + \left(\frac{\lambda_s}{\lambda}\right)^2}, \quad 2.22$$

where ϵ_0 is the static dielectric constant, ϵ_∞ is the high frequency dielectric constant, λ_s is the relaxation wavelength, or wavelength corresponding to the relaxation time, τ , and λ is the incident radiation wavelength. This theory was later expanded upon by Cole and Cole [1941] to include a spread parameter, α , whose value can vary from 0 to 1

$$\epsilon' = \epsilon_\infty + \frac{(\epsilon_0 - \epsilon_\infty) \left[1 + \left(\frac{\lambda_s}{\lambda} \right)^{1-\alpha} \sin \left(\frac{1}{2} \alpha \pi \right) \right]}{1 + 2 \left(\frac{\lambda_s}{\lambda} \right)^{1-\alpha} \sin \left(\frac{1}{2} \alpha \pi \right) + \left(\frac{\lambda_s}{\lambda} \right)^{2(1-\alpha)}} \quad 2.23$$

$$\epsilon'' = \frac{(\epsilon_0 - \epsilon_\infty) \left(\frac{\lambda_s}{\lambda} \right)^{1-\alpha} \cos \left(\frac{1}{2} \alpha \pi \right)}{1 + 2 \left(\frac{\lambda_s}{\lambda} \right)^{1-\alpha} \sin \left(\frac{1}{2} \alpha \pi \right) + \left(\frac{\lambda_s}{\lambda} \right)^{2(1-\alpha)}} + \frac{\sigma \lambda}{\sigma_0} \quad 2.24$$

The spread parameter is a measure of how the semicircular plot of ϵ' versus ϵ'' varies from the theoretical Debye equations. The equation for the loss, ϵ'' , was modified to include a frequency independent conductivity, σ :

$$\frac{\sigma \lambda}{\sigma_0} \quad 2.25$$

where $\sigma_0 = 18.8496 \times 10^{10}$ and $\sigma = 1.25664 \times 10^9$. It is important to note that when σ and λ are equal to 0, the Cole-Cole relations with the conductivity modification

reduce to the Debye equations.

The parameters, ϵ_∞ , ϵ_0 , λ_s , and α , were fit by Ray [1972] from optical constant data as a function of temperature for liquid water. These parameters are:

$$\epsilon_\infty = 5.27137 + 0.0216474T - 0.00131198T^2 \quad 2.26$$

$$\epsilon_0 = 78.54[1.0 - 4.579 \times 10^{-3}(T - 25.0) + 1.19 \times 10^{-5}(T - 25.0)^2 - 2.8 \times 10^{-8}(T - 25.0)^3] \quad 2.27$$

$$\lambda_s = 3.386 \times 10^{-4} \exp\left(\frac{2513.98}{T + 273}\right) \quad 2.28$$

$$\alpha = 0.069265 - \frac{16.8129}{T + 273}, \quad 2.29$$

where T is temperature in degrees Celsius. Since there have been no significant new measurements in the band 0.1 to 20 cm, his results will be used in the region. Data obtained at wavelengths longer than 20 cm show significant discrepancies in the imaginary part, k. After 20 cm, the wavelength dependent term, equation 2.25, begins to dominate the Cole-Cole equation for ϵ'' . The Cole-Cole equations will be used in their original format for fitting n and k for the remainder of the microwave/radiowave and the longwave regions for water. Other changes to the parameters will be discussed in the microwave/radiowave section for water of Chapter 3.

Wörz-Cole Equations

The research conducted by Wörz and Cole [1969] concentrated on ice Ih for temperatures of 0 °C to -80 °C. The E-M spectral wavelength interval associated with this study ranges from 1.5 kilometers to nearly dc. The equations used by Wörz and Cole are the Debye relaxation equations given by 2.21 and 2.22 with the frequency-independent conductivity term

$$\epsilon' = \epsilon_{\infty} + \frac{(\epsilon_0 - \epsilon_{\infty})}{1 + (\omega\tau)^2} \quad 2.30$$

$$\epsilon'' = \frac{(\epsilon_0 - \epsilon_{\infty})\omega\tau}{1 + (\omega\tau)^2} + \frac{\sigma_0}{\omega}, \quad 2.31$$

where ω is 2π frequency and τ is the relaxation time given by

$$\tau = A \exp\left(\frac{E}{kT}\right). \quad 2.32$$

$$A = 5.3 \times 10^{-6} \text{ seconds}$$

$$k = \text{Boltzman's constant} = 8.62 \times 10^{-5} \text{ eV/K}$$

$$E = \text{activation energy} = .57024 \text{ eV}$$

$$T = \text{temperature in Kelvin}$$

The conductance, σ_0 , is calculated by

$$\sigma_0 = 1.26 \exp\left(\frac{-54}{kT}\right) \quad \text{mho cm}^{-1}. \quad 2.33$$

The relation for the static and high-frequency dielectric

constants is given by

$$\varepsilon_0 - \varepsilon_\infty = \frac{20715}{T-38}, \quad 2.34$$

where T is in Kelvin and $\varepsilon_\infty = 3.1$.

The Wörz-Cole equations agree more closely with measured data for wavelengths greater than 1.5 km than do the Cole-Cole equations, perhaps due to the availability of more data. For n, the Wörz-Cole relations provide a good fit into the microwave regions.

Weighting

Some spectral intervals are comprised of two data sets. Normally for weighting, the data sets are weighted using the uncertainty or error variance, or

$$w = \frac{1}{\sigma^2}. \quad 2.35$$

where w is the weight. This weighting scheme takes on the assumption that the error follows a Gaussian distribution. Without knowledge of the statistics, this assumption cannot be made with the data sets used, and due to the disparity in measurements of similar parameters, this assumption will not be made.

In some regions, two data sets are used for fitting. Two weightings will be used for the data sets. If uncertainties are the same, an even weighting of 0.5 will be given to each set. If the uncertainties are different, an

average ratio of the total uncertainty contribution will be used. From the data sets being combined, this average is 0.7 for the data set with the lower uncertainty, and 0.3 for the data set with the higher uncertainty.

Summary

Tables 2.1 and 2.2 summarize the fitting for liquid water and ice, respectively.

Table 2.1. Methodology for water.

Real Part, n			
Interval	400 nm - 1 mm	1 mm - 20 cm	> 20 cm
Method	Cubic Splines	Cole-Cole with conductivity	Cole-Cole
Imaginary Part, k			
Interval	400 nm - 1 mm	1 mm - 20 cm	> 20 cm
Method	Cubic Splines	Cole-Cole with conductivity	Cole-Cole

Table 2.2 Methodology for ice.

Real Part, n		
Interval	400 nm - 1 mm	> 1mm
Method	Cubic Splines	Wörz-Cole
Imaginary Part, k		
Interval	400 nm - 1.5 km	> 1.5 km
Method	Cubic Splines	Wörz-Cole

CHAPTER 3

RESULTS

Introduction

The methodology outlined in Chapter 2 was applied to the data sets. Weighting was used when more than one data set was available for a spectral region. To ensure continuity between spectral regions, all attempts were made to have at least one data set span the bordering regions. This promoted a smoother connection between spectral intervals. Each interval is described as to the methodology of the fitting, data sets used, significant features, and physics of the observed features or structure. A figure of the fit along with the data used is also shown. If spline fitting is used, a table of coefficients is included.

Coefficient Equation

The cubic splines used in this study follow the format of

$$C_1 + C_2 \left(\frac{\lambda - b_j}{h} \right) + C_3 \left(\frac{\lambda - b_j}{h} \right)^2 + C_4 \left(\frac{\lambda - b_j}{h} \right)^3 \quad 3.1$$

from the interval $[b_j, b_{j+1}]$, where b_j and b_{j+1} are breakpoints, λ is the desired wavelength, h is the breakpoint width, and C_1 through C_4 are the coefficients.

To recreate the plots in this chapter, λ , in μm , is indexed through the interval of b_j to b_{j+1} . The variable, λ , is the only parameter that varies; all of the other parameters remain static throughout the interval $[b_j, b_{j+1}]$.

Each segment that is fit with cubic splines will include all variables in equation 3.1, as well as the root-mean square value for each segment. The RMS value is an indicator as to how good the splines fit the data. Generally, the fits have an RMS value less than one percent of the data values.

Water

Visible

The visible region spans the region of $0.4 \mu\text{m}$ to $0.7 \mu\text{m}$. This region was fit using cubic splines.

The measured values of n from Boguth [1973] were used for fitting the real part of the refractive index. Hale and Querry [1973] also presents data within the visible. However, a comparison of uncertainties leads to the sole selection. Boguth's measurements were taken out to 5 significant figures with an uncertainty of 1.5×10^{-3}

percent. Hale and Query's data in this region has a minimum of 0.5 percent uncertainty or a difference in two orders of magnitude. Hale and Query's data were put on the graph with uncertainty bars in Figure 3.1 for a comparison. The coefficients resulting from the fitting are given in Table 3.1.

Table 3.1. Coefficient data of water in the visible for n.

b_j	b_{j+1}	C_1	C_2	C_3	C_4	h	RMS
0.36524	0.70652	1.34655	-3.8597E-02	3.6407E-02	-1.4719E-02	0.34128	9.02E-5

Fitting the imaginary part of the refractive index in this region posed a difficult task. Two compilations of k values gave two different plots. As can be seen in Figure 3.2, the values of k given by Kopelevich [1976] are different from that of Hale and Query in some cases by an order of magnitude. Kopelevich attributes these discrepancies to the methodology employed in measuring the data compiled by Hale and Query, as was discussed in Chapter 1. The uncertainty estimates were not given by either of the authors. From investigators that included the data uncertainty, the absorption region measurements usually have a 10 percent uncertainty. However, some uncertainties are as much as ± 20 percent or as low as ± 4 percent. If

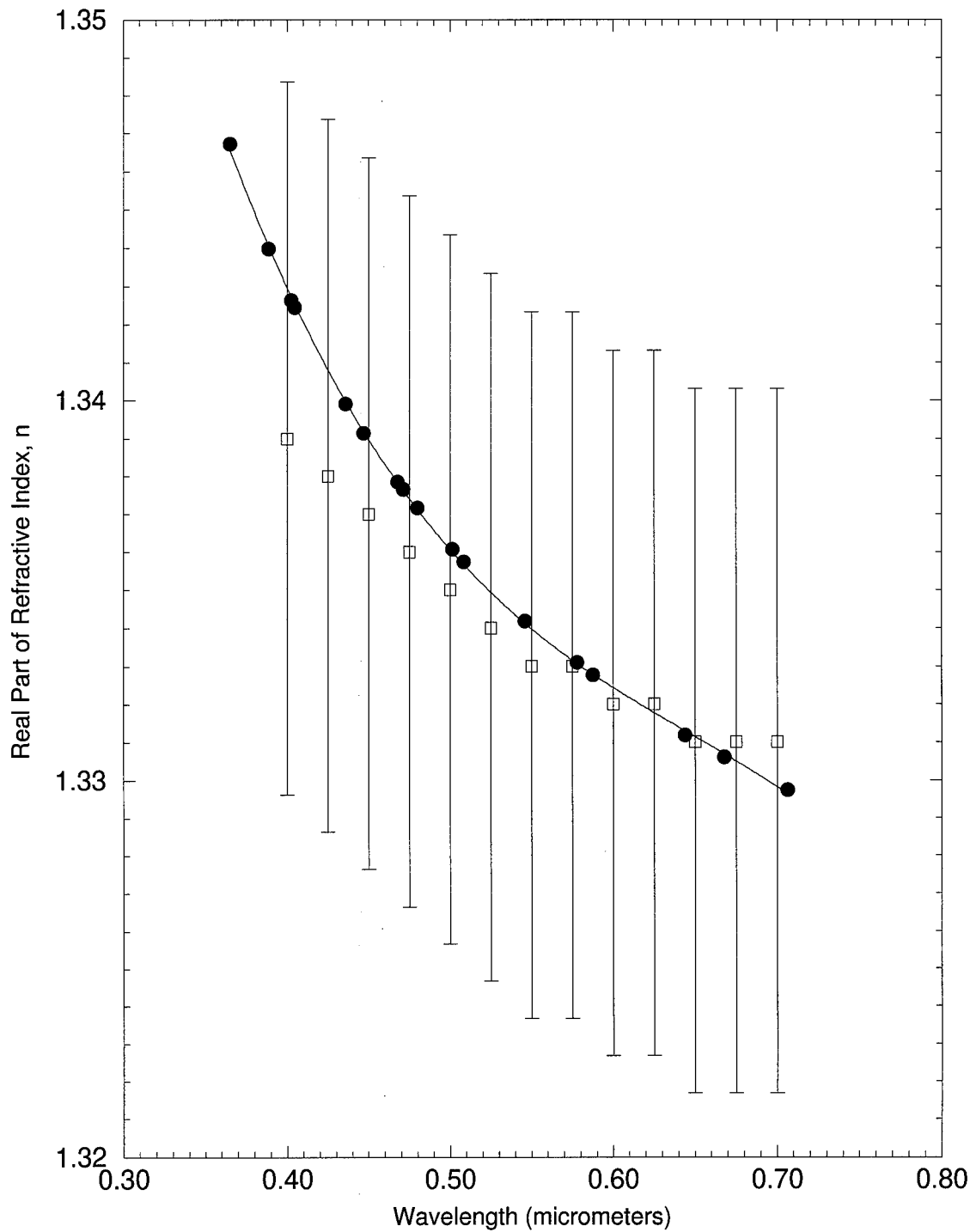


Figure 3.1. Real part of the complex index of refraction for water in the visible region. — Fitted Curve; • Boguth [1973] at 23°C; □ Hale and Query [1973] at 25°C, uncertainty of $\pm 0.7\%$.

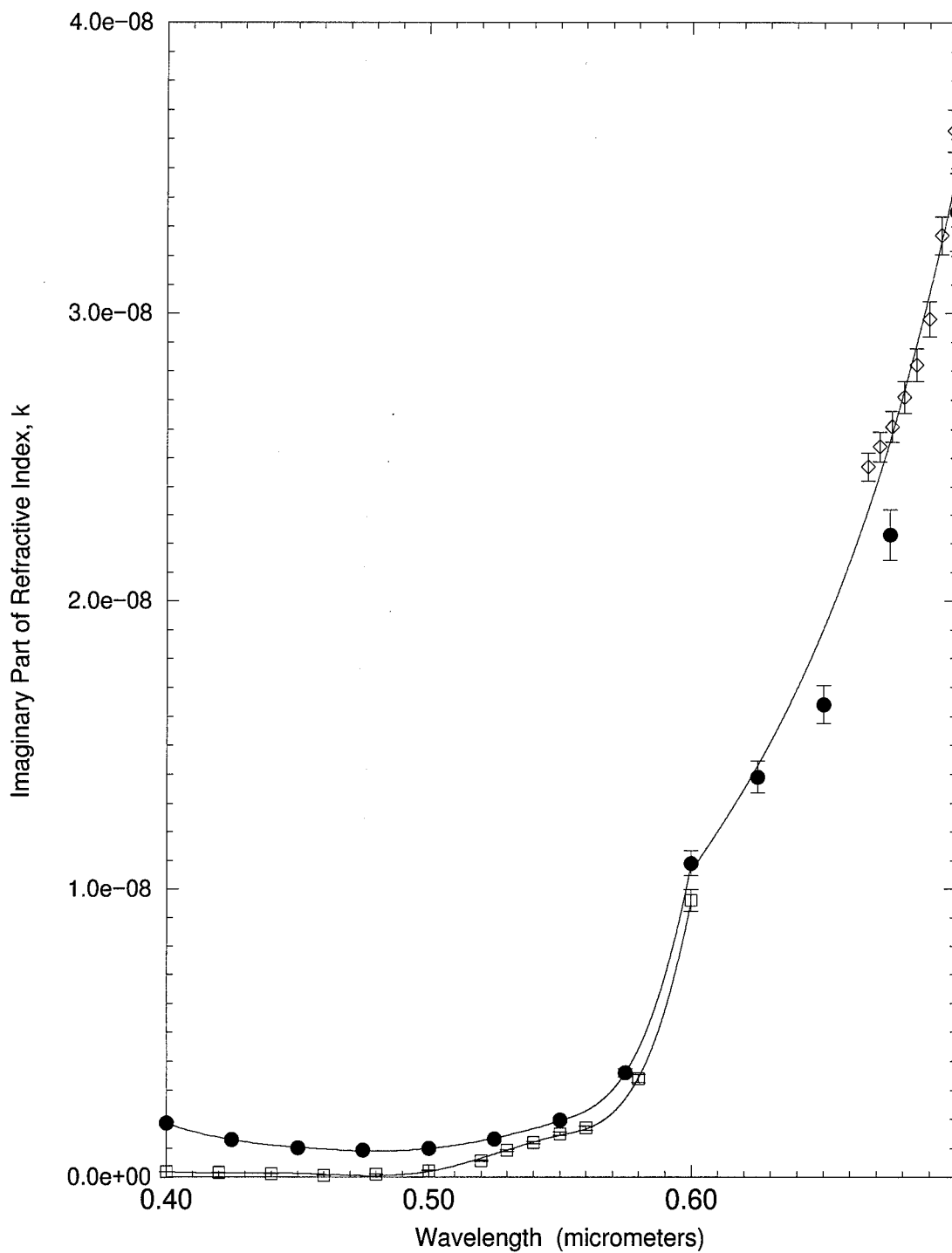


Figure 3.2. Imaginary part of the complex index of refraction for water in the visible region. — Fitted Curve; • Hale and Querry [1973] at 25°C, uncertainty of ±4%; □ Kopelevich [1976] at 20°C, uncertainty of ±4%; ◇ Kou et al. [1993] at 22°C, uncertainty of ±2%.

uncertainties were not listed, the lowest value of ± 4 percent was used, so as not to underestimate the uncertainty. An uncertainty of ± 4 percent was used with both data sets. The region of $0.4 \mu\text{m}$ to $0.6 \mu\text{m}$ was fit with each data set, and it is up to the user which methodology is more sound. The data for wavelengths longer than $0.6 \mu\text{m}$ poses a different problem. Kopelevich's tabulated values of k ends at $0.6 \mu\text{m}$, Hale and Query's k values continue on through the spectrum, and the data from Kou et al. [1992] begin at $0.65 \mu\text{m}$. Kou's k values begin with an uncertainty of 9 percent that falls to just over 5 percent in this small region. Kou et al. used a modern spectrometer at high resolution, leading to the possibility of under estimations of the uncertainties given to Kopelevich and Hale and Query's data. An attempt was made to bias this segment to Kou's data due to the improved reliability and high spectral resolution, as well as add continuity proceeding into the near infrared. Kou's data were weighted to 0.7 with the remainder to Hale and Query. The coefficients for all three segments are in Tables 3.2a, b and c.

Near Infrared

The real part of the refractive index in the near infrared region was fit with four data sets: Downing and

Table 3.2a. Coefficient data of water in the visible for k by Hale and Querry [1973] up to 0.6 μm

b_j	b_{j+1}	C_1	C_2	C_3	C_4	h	RMS
0.40	0.45	1.8608E-09	-1.5986E-09	1.0823E-09	-3.0745E-10	0.05	3.19E-11
0.45	0.50	1.0371E-09	-3.5621E-10	1.6000E-10	1.5294E-10	0.05	
0.50	0.55	9.9387E-10	4.2261E-10	6.1882E-10	-9.8836E-11	0.05	
0.55	0.60	1.9365E-09	1.3638E-09	3.2232E-10	7.2764E-09	0.05	

Table 3.2b. Coefficient data of water in the visible for k by Kopelevich [1976] up to 0.6 μm

b_j	b_{j+1}	C_1	C_2	C_3	C_4	h	RMS
0.40	0.45	1.9323E-10	-2.1995E-10	4.0347E-10	-2.3842E-10	0.05	5.4E-11
0.45	0.50	1.3834E-10	-1.2826E-10	-3.1178E-10	5.0660E-10	0.05	
0.50	0.55	2.0490E-10	7.6798E-10	1.2080E-09	-7.3464E-10	0.05	
0.55	0.60	1.4463E-09	9.8009E-10	-9.9590E-10	8.1615E-09	0.05	

Table 3.2c. Coefficient data of water in the visible for k from 0.6 μm to 0.7 μm

b_j	b_{j+1}	C_1	C_2	C_3	C_4	h	RMS
0.60	0.70	1.0631E-08	1.3485E-08	2.3055E-09	8.4117E-09	0.10	1.09E-09

Williams [1975], Palmer and Williams [1974], Hale and Querry [1973] and Zolaratev and Demin [1977]. Not all of these data sets spanned the near infrared region, for example, Palmer and Williams' data extend from 0.358 μm to 2.63 μm . This is just prior to the absorption band associated with vibrational stretching fundamentals, ν_1 and ν_3 , around 2.94 μm . There are slight temperature variations within the bands associated with these fundamentals. The temperature of 27°C lies centrally to those compared by Pinkley et al. [1977]. The temperature variation is not as significant as in other regions in the electromagnetic spectrum. Pinkley

et al. also noted a slight shift in resonant frequencies in the ν_1 and ν_3 bands as temperature varies. From 1°C to 50°C, ν_1 and ν_3 shift from 3380 cm^{-1} to 3400 cm^{-1} (2.96 μm to 2.94 μm .) All fundamentals are discussed in more detail in Appendix A.

Four segments were needed to model the behavior in the near infrared region. To obtain the best fit, four breakpoints in each segment were used. This resulted in an RMS of less than 1 percent. For the first segment, the data from Palmer and Williams, and Hale and Querry were used. This spanned wavelengths from 0.7 μm to 2.2 μm . A weight of 0.7 was given to Palmer and Williams as the uncertainty associated with their values were 1 percent versus 2 percent in Hale and Querry. The next segment ranged from 2.2 μm to 2.762 μm , and the data from Hale and Querry, and Downing and Williams were used. A weight of 0.7 was also given to Downing and Williams due to the 1 percent uncertainty in their data. The final two segments reaching to 4 μm were fit with data from Downing and Williams, and Zolaratev and Demin. Again, Downing and Williams received a weighting of 0.7 due to the uncertainty of 3 percent in Zolaratev and Demin's data. The near infrared plot for n is given in Figure 3.3 and the coefficients in Table 3.3.

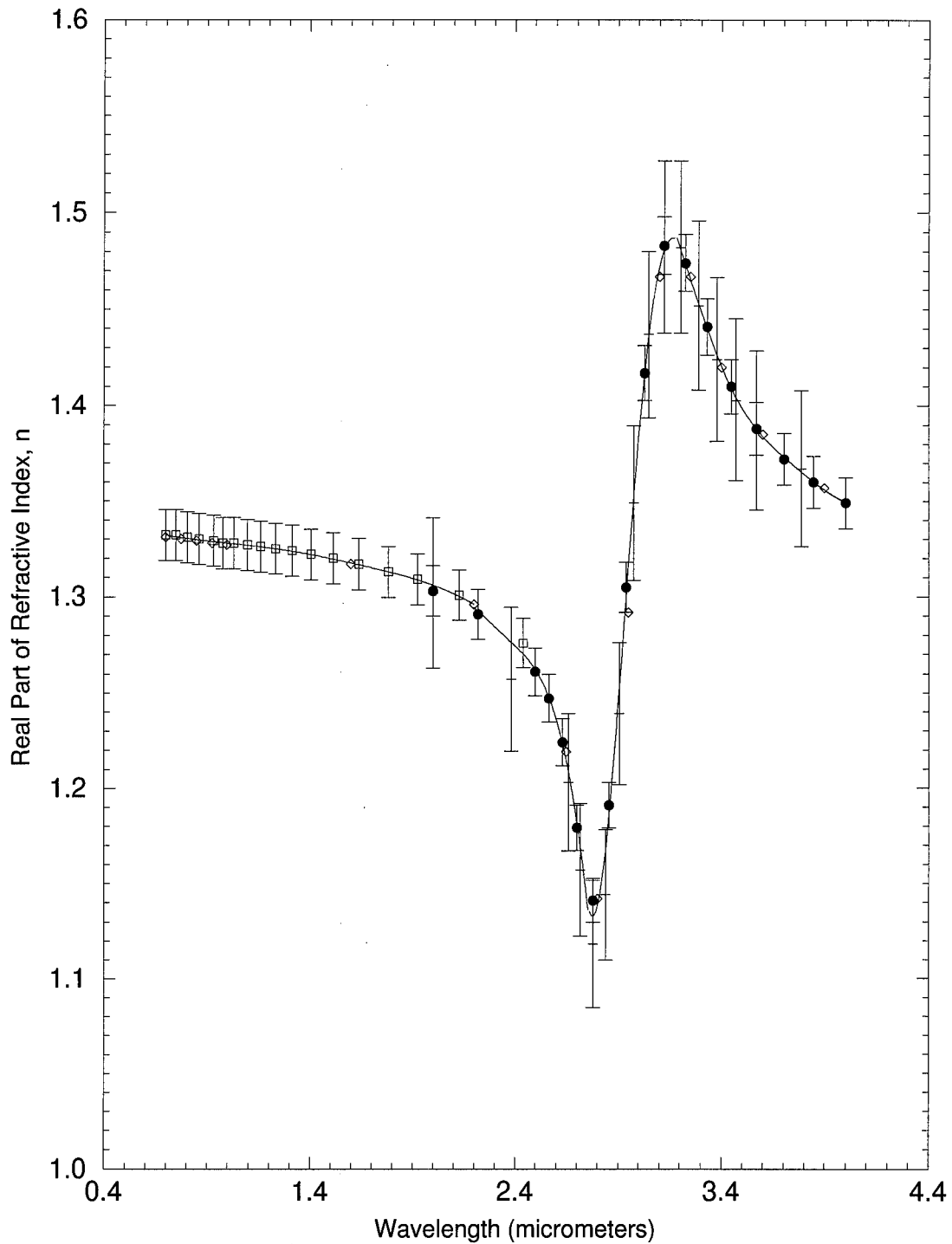


Figure 3.3. Real part of the complex index of refraction for water in the near infrared region. — Fitted Curve; • Downing and Williams [1975] at 27°C, uncertainty of $\pm 1\%$; □ Palmer and Williams [1974] at 27°C, uncertainty of $\pm 1\%$; ◇ Hale and Querry [1973] at 25°C, uncertainty of $\pm 2\%$; + Zolaratev and Demin [1977] at 25°C, uncertainty of $\pm 3\%$.

Table 3.3. Coefficient data of water in the near infrared for n.

b_j	b_{j+1}	C_1	C_2	C_3	C_4	h	RMS
0.70000	1.20000	1.3320900	-1.0216E-02	7.5652E-03	-4.0020E-03	0.500000	6.16E-04
1.20000	1.70000	1.3254400	-7.0915E-03	-4.4408E-03	1.1937E-03	0.500000	
1.70000	2.20000	1.3151000	-1.2392E-02	-8.5962E-04	-5.5889E-03	0.500000	
2.20000	2.38493	1.2944900	-1.6593E-02	-3.6562E-03	1.8005E-03	0.184933	3.55E-03
2.38493	2.56987	1.2760400	-1.8504E-02	1.7453E-03	-1.3083E-02	0.184933	
2.56987	2.76200	1.2462000	-5.4262E-02	-3.7503E-02	-1.9138E-02	0.184933	
2.76200	2.89953	1.1353900	-4.5099E-02	2.1464E-01	-6.3250E-02	0.137533	8.31E-03
2.89953	3.03707	1.2416800	1.9443E-01	2.4888E-02	-3.5658E-02	0.137533	
3.03707	3.17500	1.4253400	1.3723E-01	-8.2085E-02	6.3402E-03	0.137533	
3.17500	3.45647	1.4869000	-8.9269E-02	-1.2811E-03	1.1165E-02	0.271767	1.29E-3
3.45647	3.72823	1.4075100	-5.8337E-02	3.2214E-02	-1.0553E-02	0.271767	
3.72823	4.00000	1.3708400	-2.5567E-02	5.5611E-04	3.6075E-03	0.271767	

The imaginary part proved to be more difficult due to the complexity of the absorption bands. The interval between 0.7 μm to 2.222 μm needed 8 segments encompassing 29 splines. This was needed to preserve the minor absorption peaks. The data from Kou et al. [1992] were weighted 0.7. Hale and Query [1973] was also used in this region receiving the remainder of the weight. The remainder of the band was fit using Downing and Williams [1975], and Hale and Query with equal weighting due to the same uncertainties.

Pinkley et al. [1976] have shown a greater temperature dependence in the ν_1 , ν_3 fundamentals. The 22 percent difference discussed was from 1°C to 50°C. For meteorological applications, a more meaningful comparison is between 1°C and 27°C, which results in a 12.5 percent difference. The paucity of data spanning the temperature

range precludes deriving a temperature dependence coefficient. This temperature variation should be considered if higher precision is needed.

The largest peak, around 2.94 μm , is associated with the stretching fundamentals. The minor absorption bands centered at 1.9 μm and 1.5 μm are associated with combinational bands as proposed by Pinkley et al. The wavelengths in their study for these fundamentals, however, do not match those as shown in Figure 3.4. The coefficients for the fit can be found in Table 3.4.

Middle Infrared

The middle infrared encompassed the spectral interval from 4 μm to 50 μm . The real and imaginary parts were both fit with data from Downing and Williams [1975] and Zolaratev and Demin [1977]. For the real part, emphasis was placed on Downing and William's data due to the lesser uncertainty warranting a weight of 0.7. Five segments containing a total of 17 splines were needed to produce the fit given in Figure 3.5. The coefficients are provided in Table 3.5.

The data used to fit the imaginary part were equally weighted due to the assumption that they all were characterized by the same uncertainty. The additional complexity of the curve required additional splines to model. Six segments with 24 splines were needed to model

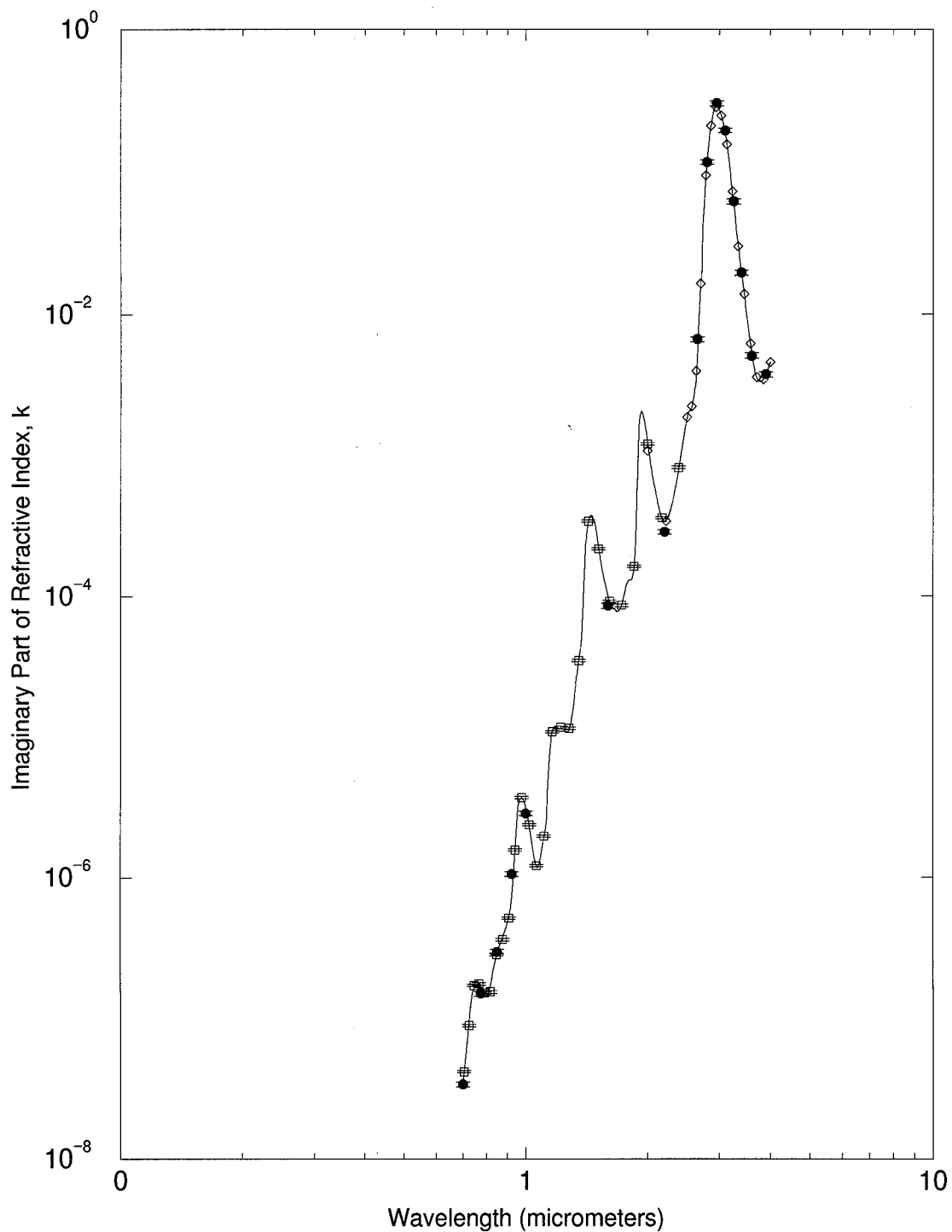


Figure 3.4. Imaginary part of the complex index of refraction for water in the near infrared region. — Fitted Curve; • Hale and Querry [1973] at 25°C, uncertainty of $\pm 4\%$; □ Kou et al. [1993] at 22°C, uncertainty of $\pm 2\%$; ◇ Downing and Williams [1975] at 27°C, uncertainty of $\pm 4\%$.

Table 3.4. Coefficient data of water in the near infrared for k.

b_j	b_{j+1}	C_1	C_2	C_3	C_4	h	RMS
0.70000	0.75158	3.5184E-08	1.3664E-08	3.2839E-07	-2.0046E-07	5.158E-02	5.6E-08
0.75158	0.80316	1.7678E-07	6.9068E-08	-2.7299E-07	1.6867E-07	5.158E-02	
0.80316	0.85474	1.4153E-07	2.9103E-08	2.3302E-07	-1.0605E-07	5.158E-02	
0.85474	0.90632	2.9761E-07	1.7700E-07	-8.5126E-08	1.0688E-07	5.158E-02	
0.90632	0.95790	4.9636E-07	3.2738E-07	2.3550E-07	2.1925E-06	5.158E-02	
0.95790	1.01063	3.2400E-06	3.1200E-06	-5.3500E-06	1.7900E-06	5.270E-02	3.8E-08
1.01063	1.06337	2.8000E-06	-2.2200E-06	1.3200E-08	6.0900E-07	5.270E-02	
1.06337	1.11610	1.2000E-06	-3.6500E-07	1.8400E-06	-5.5100E-07	5.270E-02	
1.11610	1.15777	2.0800E-06	-2.0200E-06	2.0100E-05	-1.0000E-05	4.170E-02	3.6E-07
1.15777	1.19943	1.0100E-05	7.9700E-06	-1.0100E-05	3.8000E-06	4.170E-02	
1.19943	1.24110	1.1800E-05	-7.5000E-07	1.3400E-06	-9.0200E-07	4.170E-02	
1.24110	1.28277	1.1500E-05	-7.6700E-07	-1.3600E-06	2.1100E-06	4.170E-02	
1.28277	1.32443	1.1500E-05	2.8500E-06	4.9700E-06	1.6000E-06	4.170E-02	
1.32443	1.36610	2.0900E-05	1.7600E-05	9.7600E-06	-5.6600E-06	4.170E-02	
1.36610	1.40850	4.3400E-05	1.1300E-05	1.3100E-04	6.6800E-05	4.240E-02	1.3E-05
1.40850	1.46238	2.5100E-04	3.3800E-04	-2.4500E-04	2.6300E-05	5.390E-02	2.9E-06
1.46238	1.51626	3.7000E-04	-7.3200E-05	-1.6600E-04	8.3800E-05	5.390E-02	
1.51626	1.57014	2.1500E-04	-1.5400E-04	8.5400E-05	-2.3700E-05	5.390E-02	
1.57014	1.62402	1.2300E-04	-5.4400E-05	1.4100E-05	3.1800E-06	5.390E-02	
1.62402	1.67790	8.5700E-05	-1.6600E-05	2.3600E-05	-1.6000E-05	5.390E-02	
1.67790	1.73590	7.8400E-05	-4.6700E-06	1.5600E-05	3.5000E-06	5.800E-02	3.5E-06
1.73590	1.79390	9.2800E-05	3.6900E-05	2.6100E-05	-2.5900E-05	5.800E-02	
1.79390	1.85190	1.3000E-04	1.1500E-05	-5.1500E-05	7.3600E-05	5.800E-02	
1.85190	1.88680	1.6400E-04	1.3300E-04	-1.0200E-04	5.3600E-04	3.490E-02	1.1E-06
1.88680	1.95388	6.7400E-04	5.1200E-03	-5.7400E-03	1.8300E-03	6.710E-02	2.4E-05
1.95388	2.02096	1.8900E-03	-8.6700E-04	-2.5400E-04	2.2200E-04	6.710E-02	
2.02096	2.08804	9.8900E-04	-7.0900E-04	4.1300E-04	-1.2400E-04	6.710E-02	
2.08804	2.15512	5.6900E-04	-2.5500E-04	4.0400E-05	2.1900E-05	6.710E-02	
2.15512	2.22220	3.7600E-04	-1.0900E-04	1.0600E-04	-2.3000E-05	6.710E-02	
2.22220	2.50000	3.5100E-04	1.6700E-04	6.9100E-04	7.0100E-04	2.778E-01	1.8E-05
2.50000	2.55435	1.8500E-03	1.1700E-03	-1.7500E-03	8.5500E-04	5.440E-02	6.6E-04
2.55435	2.60870	2.1300E-03	2.3100E-04	8.1000E-04	-2.1300E-04	5.440E-02	
2.60870	2.66305	2.9600E-03	1.2100E-03	1.7200E-04	2.7600E-03	5.440E-02	
2.66305	2.71740	7.1000E-03	9.8400E-03	8.4500E-03	-4.6200E-03	5.440E-02	
2.71740	2.81450	1.9300E-02	1.2777E-01	-3.5500E-02	2.7200E-02	9.710E-02	3.5E-03
2.81450	2.91160	1.3881E-01	1.3843E-01	4.6200E-02	-5.2600E-02	9.710E-02	
2.91160	3.00870	2.7078E-01	7.2900E-02	-1.1174E-01	2.8400E-02	9.710E-02	
3.00870	3.10580	2.6034E-01	-6.5300E-02	-2.6400E-02	7.0300E-03	9.710E-02	
3.10580	3.20290	1.7561E-01	-9.7100E-02	-5.3600E-03	1.3200E-02	9.710E-02	
3.20290	3.30000	8.6300E-02	-6.8400E-02	3.4100E-02	-1.5300E-02	9.710E-02	
3.30000	3.53333	3.7300E-02	-5.4700E-02	3.2900E-02	-7.6500E-03	2.333E-01	3.1E-04
3.53333	3.76667	7.9300E-03	-1.1700E-02	9.9800E-03	-2.7700E-03	2.333E-01	
3.76667	4.00000	3.3900E-03	-1.0100E-04	1.6700E-03	-3.0800E-04	2.333E-01	

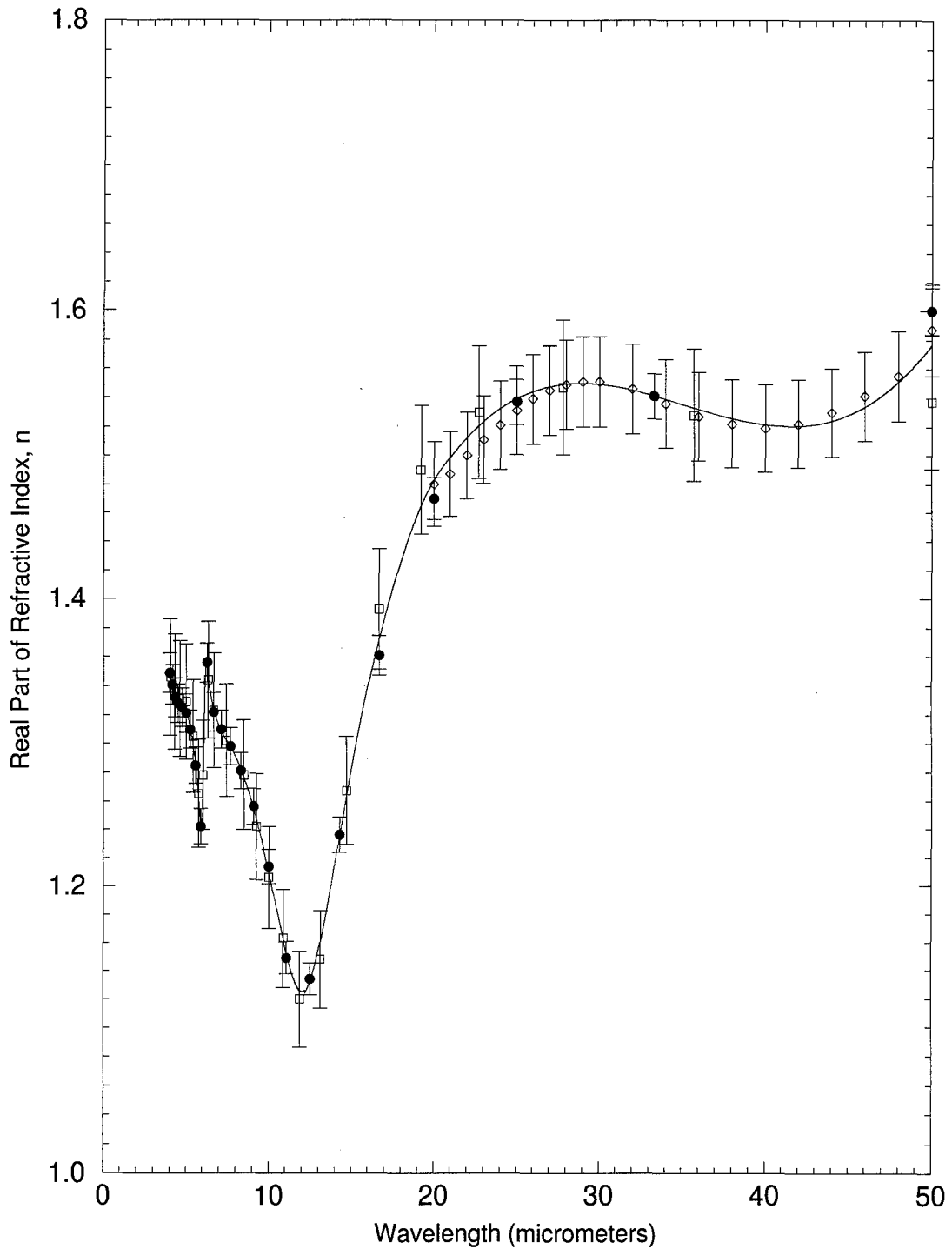


Figure 3.5. Real part of the complex index of refraction for water in the middle infrared region. — Fitted Curve; • Downing and Williams [1975] at 27°C, uncertainty of $\pm 1\%$; □ Zolaratev and Demin [1977] at 25°C, uncertainty of $\pm 3\%$; ◇ Hale and Query [1973] at 25°C, uncertainty of $\pm 2\%$.

Table 3.5. Coefficient data of water in the middle infrared for n.

b_j	b_{j+1}	C_1	C_2	C_3	C_4	h	RMS
4.00000	4.27389	1.34863	-1.0840E-02	-6.0220E-03	3.7997E-03	0.27389	2.37E-03
4.27389	4.54777	1.33556	-1.1485E-02	5.3772E-03	-1.0379E-03	0.27389	
4.54777	4.82166	1.32842	-3.8440E-03	2.2635E-03	-1.2593E-03	0.27389	
4.82166	5.09554	1.32558	-3.0948E-03	-1.5143E-03	-1.5490E-03	0.27389	
5.09554	5.36943	1.31942	-1.0770E-02	-6.1613E-03	1.3152E-03	0.27389	
5.36943	5.64331	1.30381	-1.9148E-02	-2.2160E-03	-4.5366E-03	0.27389	
5.64331	5.91720	1.27790	-3.7190E-02	-1.5826E-02	1.4098E-02	0.27389	
5.91720	6.25000	1.24162	-3.9052E-02	5.0951E-01	-3.5809E-01	0.33280	4.74E-03
6.25000	7.73627	1.35221	-1.2664E-01	1.1642E-01	-4.5300E-02	1.48627	2.81E-03
7.73627	9.22255	1.29665	-2.9800E-02	-1.9600E-02	9.7500E-04	1.48627	
9.22255	10.70880	1.24820	-6.6100E-02	-1.6700E-02	6.5000E-03	1.48627	
10.70880	12.19510	1.17191	-8.0000E-02	2.8300E-03	3.1300E-02	1.48627	
12.19510	14.79670	1.12392	5.0900E-02	1.6426E-01	-6.9900E-02	2.60163	1.26E-02
14.79670	17.39840	1.26925	1.6984E-01	-4.5400E-02	8.8100E-03	2.60163	
17.39840	20.00000	1.40252	1.0553E-01	-1.8900E-02	-6.9000E-03	2.60163	
20.00000	35.00000	1.48291	2.6192E-01	-3.1349E-01	1.0400E-01	15.00000	8.72E-03
35.00000	50.00000	1.53555	-5.2400E-02	-8.4400E-04	9.4300E-02	15.00000	

this region. The fit is given in Figure 3.6 and the associated coefficients for the splines in Table 3.6.

The absorption band around 6.1 μm is associated with the ν_2 , or bending, fundamental. Further into the middle infrared region, a broad absorption band peaks in the region of 17 μm . This is associated with the ν_L , or librational, mode as given by Franks [1972].

The temperature dependence associated with these fundamentals is very weak. Pinkley et al. [1977] has shown that the libration mode shifts very little from 1°C to 27°C. The shift is from 590 cm^{-1} to 570 cm^{-1} (16.95 μm to 17.54 μm .)

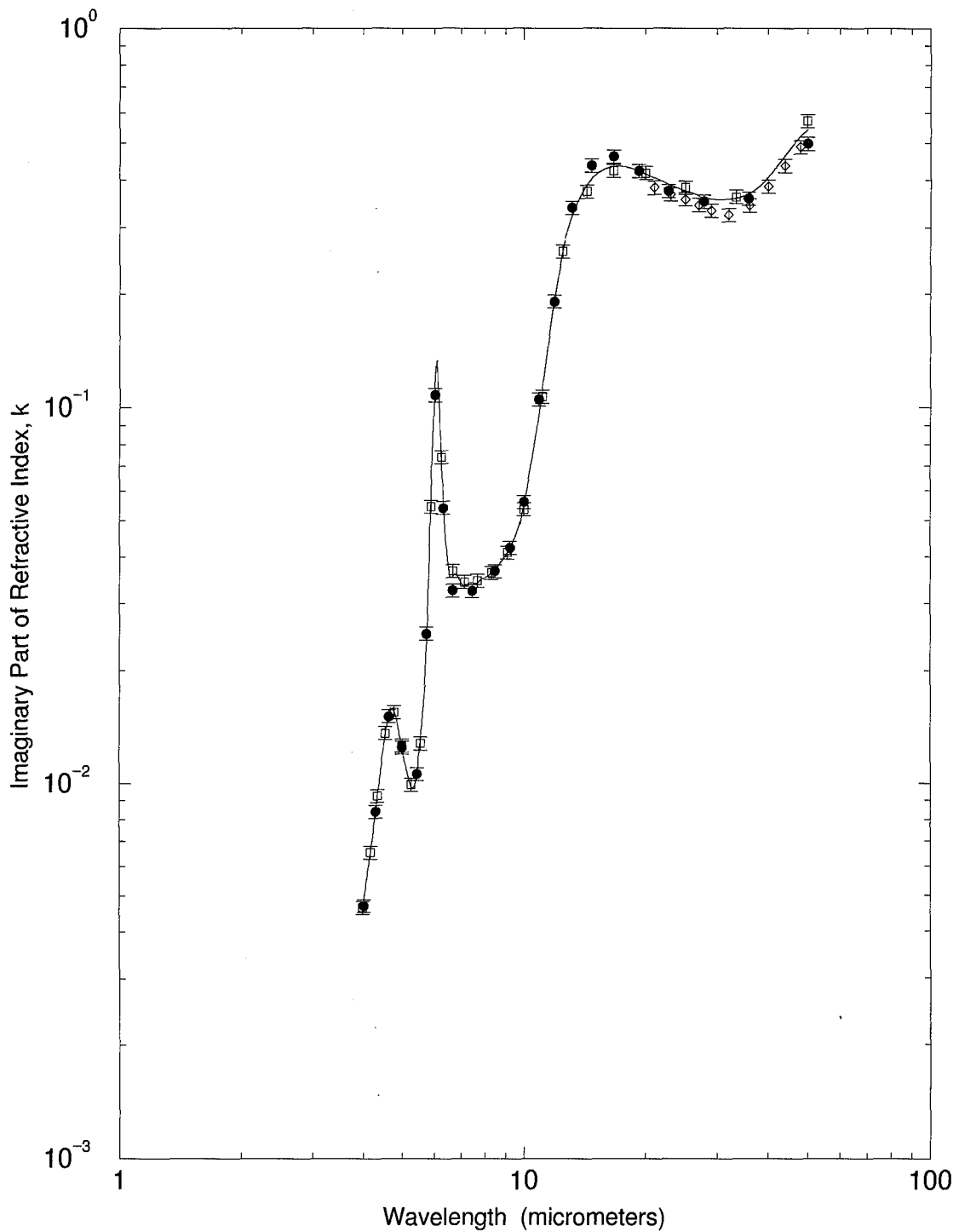


Figure 3.6. Imaginary part of the complex index of refraction for water in the middle infrared region. — Fitted Curve; • Zolaratev and Demin [1977] at 25°C, uncertainty of $\pm 4\%$; □ Downing and Williams [1975] at 27°C, uncertainty of $\pm 4\%$; ◇ Hale and Querry [1973] at 25°C, uncertainty of $\pm 4\%$.

The continuum, also, is apparent in the 8.5 μm to 12.5 μm range. In this region, there is a marked decrease in n , as well as k .

Table 3.6. Coefficient data of water in the middle infrared for k .

b_j	b_{j+1}	C_1	C_2	C_3	C_4	h	RMS
4.00000	4.23307	4.5664E-03	2.6395E-03	-3.2914E-04	4.7954E-04	0.23307	9.35E-04
4.23307	4.46613	7.3563E-03	3.4199E-03	1.1095E-03	-1.4801E-04	0.23307	
4.46613	4.69920	1.1738E-02	5.1948E-03	6.6547E-04	-1.8776E-03	0.23307	
4.69920	4.93227	1.5720E-02	8.9305E-04	-4.9673E-03	1.8099E-03	0.23307	
4.93227	5.16533	1.3456E-02	-3.6118E-03	4.6243E-04	1.7396E-04	0.23307	
5.16533	5.39840	1.0481E-02	-2.1651E-03	9.8432E-04	8.3162E-04	0.23307	
5.39840	5.63147	1.0132E-02	2.2984E-03	3.4792E-03	-2.3671E-05	0.23307	
5.63147	5.86453	1.5886E-02	9.1858E-03	3.4082E-03	2.0703E-02	0.23307	
5.86453	6.09760	4.9182E-02	7.8110E-02	6.5517E-02	-5.9307E-02	0.23307	
6.09760	6.41467	1.3348E-01	-1.6039E-01	8.4500E-02	-1.4000E-02	0.31707	2.42E-03
6.41467	6.73173	4.3500E-02	-3.3500E-02	4.2400E-02	-1.6600E-02	0.31707	
6.73173	7.04880	3.5800E-02	1.4100E-03	-7.4700E-03	3.9100E-03	0.31707	
7.04880	7.36587	3.3700E-02	-1.7900E-03	4.2600E-03	-2.0900E-03	0.31707	
7.36587	7.68293	3.4000E-02	4.6900E-04	-2.0000E-03	1.4900E-03	0.31707	
7.68293	8.00000	3.4000E-02	9.3000E-04	2.4600E-03	-2.6500E-03	0.31707	
8.00000	8.90195	3.5100E-02	1.5700E-03	4.0500E-03	-1.1900E-03	0.90195	2.43E-04
8.90195	9.80390	3.9600E-02	6.1200E-03	4.9300E-04	3.4300E-03	0.90195	
9.80390	11.23110	4.8700E-02	4.1700E-02	1.1300E-02	1.9900E-02	1.42715	4.75E-03
11.23110	12.65820	1.2155E-01	1.2397E-01	7.1000E-02	-3.8400E-02	1.42715	
12.65820	16.25040	2.8197E-01	3.3051E-01	-2.3999E-01	5.9100E-02	3.59220	1.47E-02
16.25040	19.84260	4.3156E-01	2.7700E-02	-6.2800E-02	2.0600E-02	3.59220	
19.84260	23.43480	4.1708E-01	-3.6100E-02	-1.0400E-03	4.1500E-03	3.59220	
23.43480	27.02700	3.8409E-01	-2.5700E-02	1.1400E-02	-5.6500E-03	3.59220	
27.02700	38.51350	3.6196E-01	-3.5900E-02	3.8700E-02	2.5400E-02	11.48650	1.47E-02
38.51350	50.00000	3.9017E-01	1.1776E-01	1.1500E-01	-8.1200E-02	11.48650	

Far Infrared

The far infrared region encompasses those wavelengths between 50 μm to 1000 μm . This region posed difficulties for modeling. The data are sparse from 200 μm to the end of

the spectral interval. The far infrared region also contains the onset of the broad temperature dependent hindered translation bands.

The fitting in this region used data from Downing and Williams [1975], and Afsar and Hasted [1978]. The data were close in measurement temperature, 27°C and 30°C, respectively. The data for the real part of the refractive index are close in agreement, however, the data for the imaginary part differ by more than 15 percent at 250 μm . Afsar and Hasted's data was compared to data compiled by Zolaratev and Demin [1977] at 25 °C. This comparison shows a deviation as low as 2 percent at 250 μm , but one as high as 27 percent at 1000 μm . The temperature dependence is well known, but judging by the variations in measurements, it is not well described quantitatively. These large discrepancies of the data do not prove beneficial for possible improvements in the Cole-Cole parameters, or any other derivation of temperature dependent relations. The fit is illustrated in Figures 3.7 and 3.8 for n and k , respectively. The coefficients are contained in Tables 3.7 and 3.8.

In the far infrared region, two fundamentals are apparent. The rotation or libration fundamental peaks at

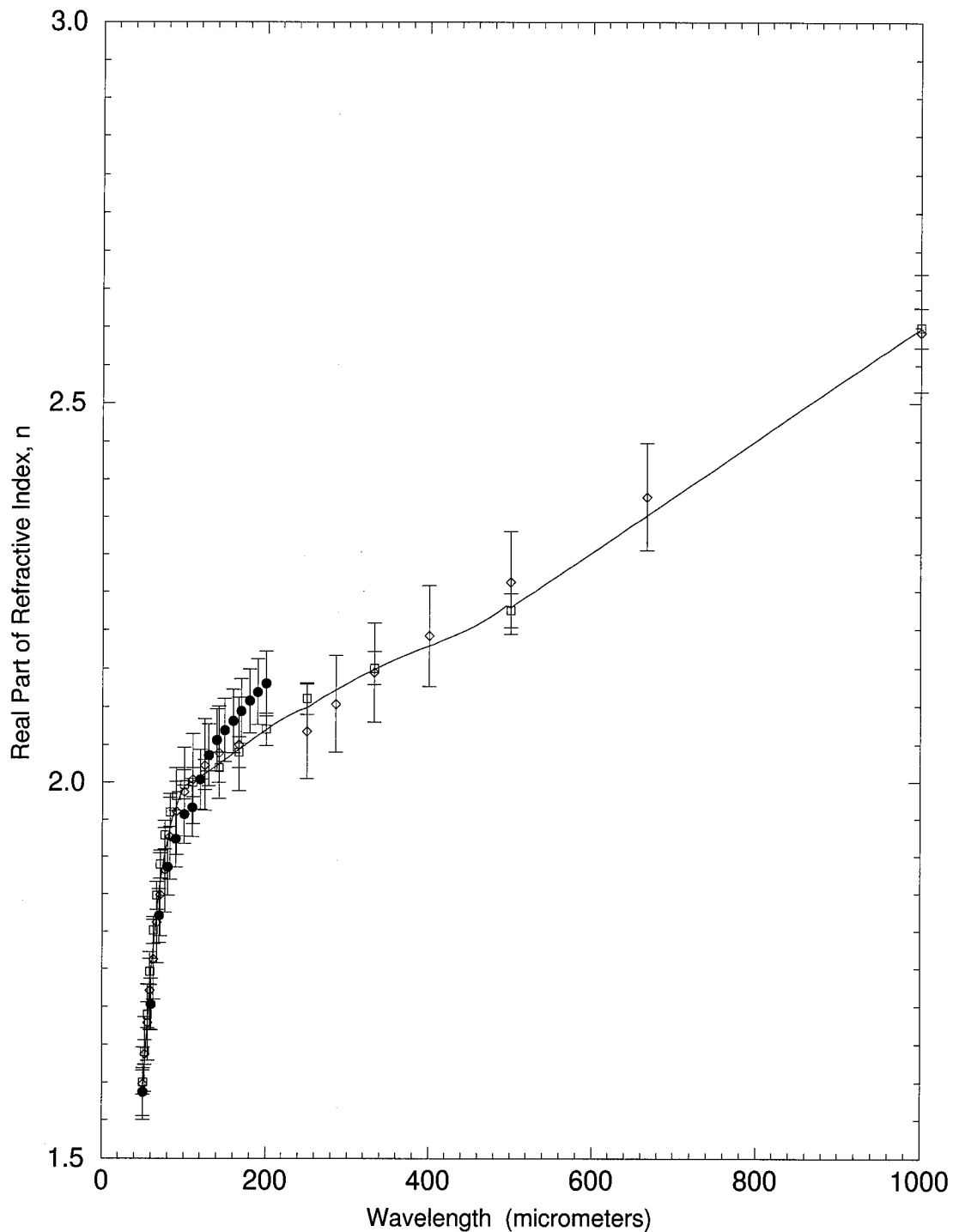


Figure 3.7. Real part of the complex index of refraction for water in the far infrared region. — Fitted Curve; • Hale and Querry [1973] at 25°C, uncertainty of $\pm 2\%$; □ Downing and Williams [1975] at 27°C, uncertainty of $\pm 1\%$; ◇ Afsar and Hasted [1978] at 30°C, uncertainty of $\pm 3\%$.

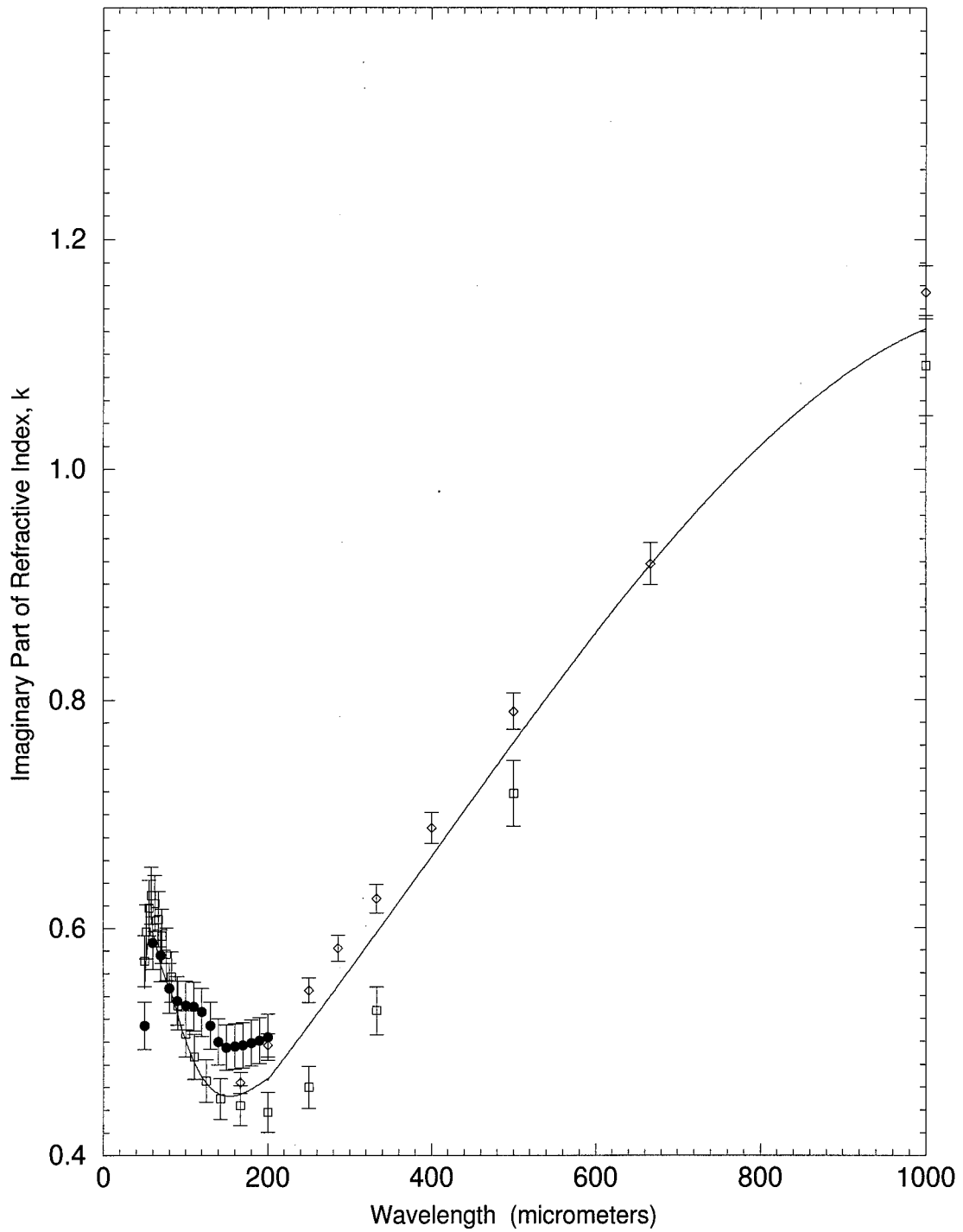


Figure 3.8. Imaginary part of the complex index of refraction for water in the far infrared region. — Fitted Curve; • Hale and Querry [1973] at 25°C, uncertainty of $\pm 4\%$; □ Downing and Williams [1975] at 27°C, uncertainty of $\pm 4\%$; ◇ Afsar and Hasted [1978] at 30°C, uncertainty of $\pm 2\%$.

around 58.8 μm . Much of the remainder of the spectrum is dominated by hindered translational modes, or as Franks [1972] describes, as hydrogen bond bending and stretching.

Table 3.7. Coefficient data of water in the far infrared for n.

b_j	b_{j+1}	C_1	C_2	C_3	C_4	h	RMS
50	75	1.59438	4.5292E-01	-1.7228E-01	2.1370E-02	25	1.65E-02
75	100	1.89639	1.7248E-01	-1.0817E-01	3.1825E-02	25	
100	250	1.99508	8.5500E-02	8.3100E-02	-6.5100E-02	150	5.48E-03
250	375	2.09830	8.5400E-02	-1.4000E-02	-1.1200E-03	125	6.09E-03
375	500	2.16859	5.4100E-02	-1.7300E-02	3.0200E-02	125	
500	1000	2.22916	3.5405E-01	3.9400E-02	-2.4200E-02	500	4.40E-03

Table 3.8. Coefficient data of water in the far infrared for k.

b_j	b_{j+1}	C_1	C_2	C_3	C_4	h	RMS
50.0000	66.6667	0.546968	0.2299390	-0.3173530	0.1173440	16.6667	2.68E-02
66.6667	83.3333	0.576899	-0.0527335	0.0346798	-0.0175368	16.6667	
83.3333	100.0000	0.541308	-0.0359845	-0.0179307	0.0146772	16.6667	
100.0000	200.0000	0.502060	-0.2153310	0.2824840	-0.1020000	100.0000	7.55E-03
200.0000	1000.0000	0.466786	0.7485750	0.2241440	-0.3173450	800.0000	3.90E-02

Microwave/Radiowave

The microwave/radiowave region is defined as the wavelengths between 1mm and 100 meters. Ray [1972] heavily investigated portions of this region using the Cole-Cole equations, 2.23 and 2.24, with the term given in equation 2.25. The Cole-Cole equations begin to depart from measured data at wavelengths less than 3 mm. Afsar and Hasted [1978] noted this in their measurements. The temperature dependent

parameters deviate from measured values at the onset of the far infrared. There have been no new broadband measurements in the region of 1 mm to 10 cm with varied temperatures to warrant a recalibration of the parameters proposed by Ray. This region is highly temperature dependent, so equations describing the physical processes are necessary. For this, Ray's parameters with the Cole-Cole equations were used to fit down to 1 mm. Because of the use of the Cole-Cole equations and the deviation the data have shown, it will be expected not to have a smooth transition between the far infrared into the microwave regions. A trade off must be made to have equations that produce temperature-dependent values. If updated measurements are made in this region for a span of temperatures, the parameters could, perhaps, be adjusted in order to provide a more accurate fit. A slightly more accurate equation of the static dielectric equation was used from Malmberg and Maryott [1956], claiming a 0.1 percent uncertainty.

$$\epsilon = 87.740 - 0.4008t + 9.398 \times 10^{-4}t^2 - 1.410 \times 10^{-6}t^3. \quad 3.2$$

The variable t in equation 3.2 is temperature in degrees Celsius. Data from Schwan et al. [1976], Grant and Sheppard [1974], and Sheppard [1973] showed a large deviation between the Cole-Cole equations using the conductivity term. The data exhibits a downward trend, while the equations produce

an increasing value with increasing wavelength. After approximately 20 cm, the wavelength-dependent conductivity term begins to dominate the expression. The result is an unrealistic increase in both n and k , with increasing wavelengths. Removing the conductivity term for wavelengths longer than 20 cm produces a downward trend for the remainder of this spectral region.

The plots in Figure 3.9 show the n and k curves plotted using the Cole-Cole equations. The wavelength dependent term was used during the peak in the hindered translation mode around 1 cm. For wavelengths greater than 20 cm, this term was removed to produce the correct longwave behavior for water. These plots were made for a temperature of 27 °C. The data from Schwan et al. show good agreement as their measurements were made at 25 °C. Both of the other data sets were made at 4 °C and were included to show the magnitude of temperature dependence in this region.

Longwave

The longwave region corresponds to wavelengths greater than 100 meters. The real and imaginary parts were fit with the Cole-Cole equations, 2.23 and 2.24, using the parameters proposed by Ray [1972] and the static dielectric constant proposed by Malmberg and Maryott [1956]. The plots in Figure 3.10 show a flat line n as it has reached the steady

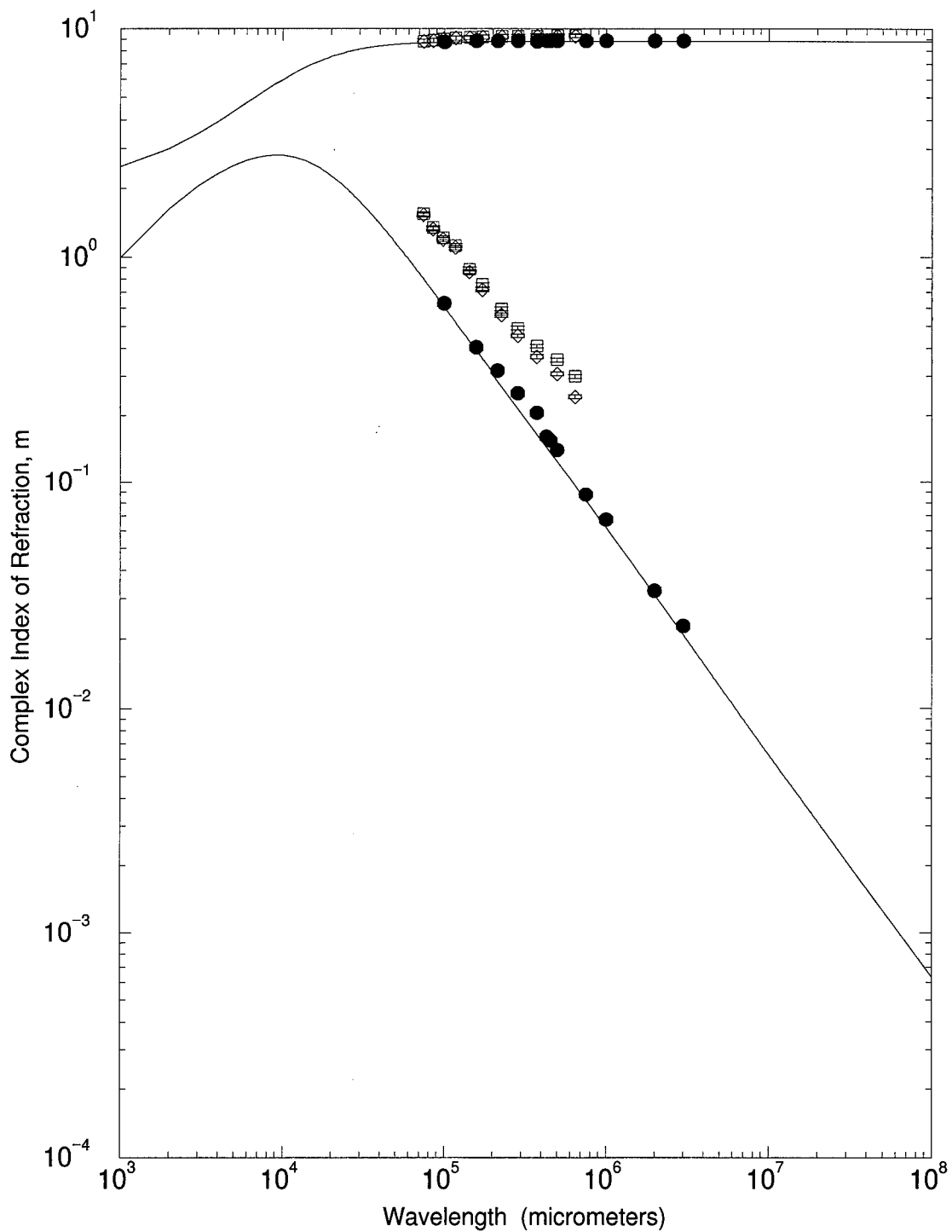


Figure 3.9. Complex indices of refraction for water in the microwave/radiowave region. — Calculated n (top) and k (bottom); • Schwan et al. [1976] at 25°C, uncertainty of $\pm 1\%$ for n and $\pm 3\%$ for k ; □ Sheppard [1973] at 4°C, uncertainty of $\pm 1\%$ for n and $\pm 3\%$ for k ; ◇ Grant and Sheppard [1974] at 4°C, uncertainty of $\pm 1\%$ for n and $\pm 3\%$ for k .

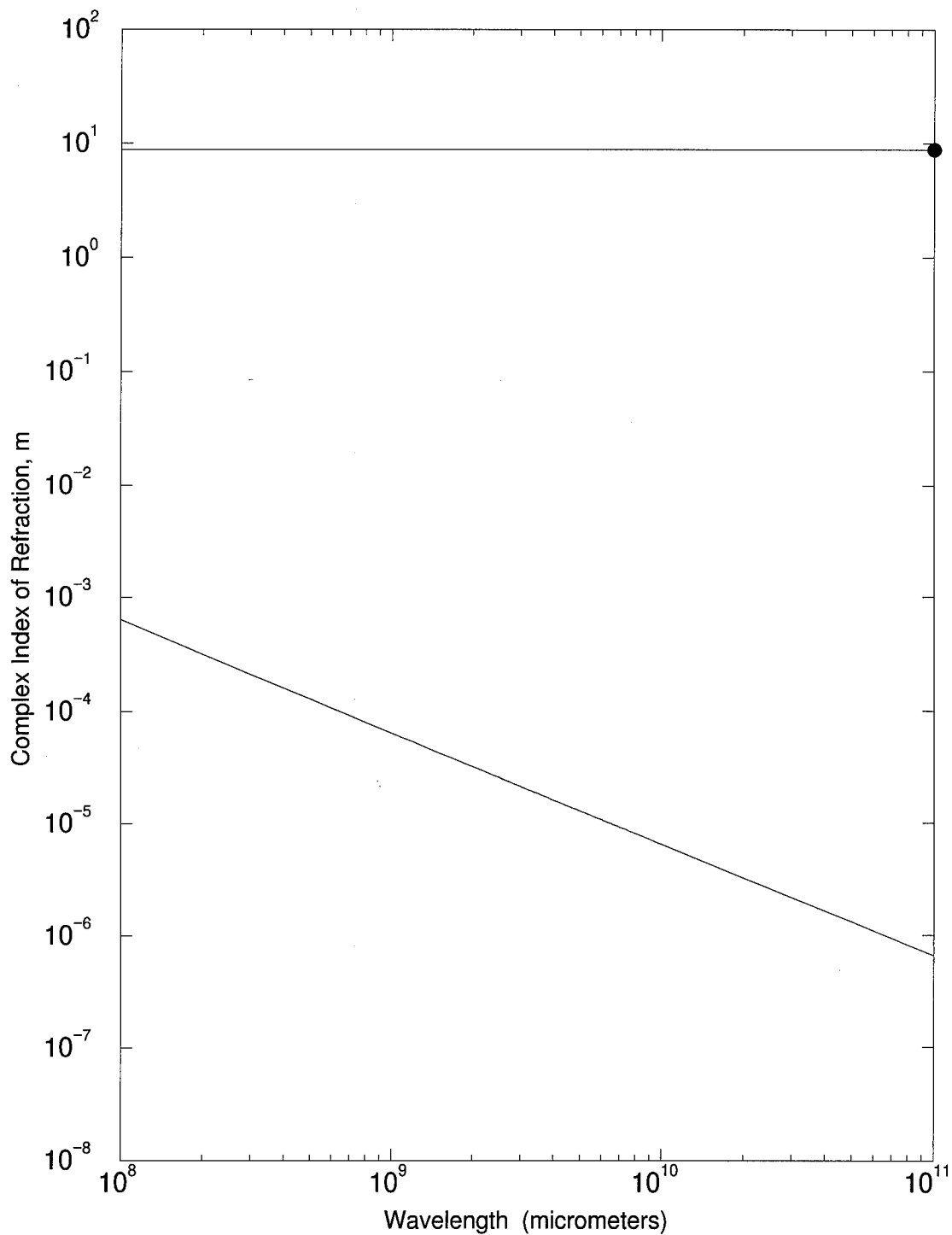


Figure 3.10. Complex indices of refraction for water in the longwave region. — Calculated n (top) and k (bottom); • Malmberg and Maryott [1956] at 25°C, uncertainty of $\pm 0.6\%$ for n.

state value of approximately 8.8. The value of k monotonically declines to essentially zero. The real part meets the value measured by Malmberg and Maryott at a wavelength of 100 km. Authors such as Malmberg and Maryott have shown temperature dependence of the permittivity in the longwave region.

Summary

The fitted curve to the real and imaginary parts of the refractive index are presented in Figure 3.11 for water over the entire spectrum discussed. The temperature for this plot is 25°C.

Ice

Visible

For the visible region, the data from Warren [1984] were used. Only one spline was needed for both the real and imaginary parts. The plots for the n and k curves are given in Figures 3.12 and 3.13, respectively. The coefficients are in Tables 3.9 and 3.10, respectively. The uncertainties in Warren's data were taken to be ± 0.1 percent for the real and ± 10 percent for the imaginary.

Table 3.9. Coefficient data of ice in the visible for n .

b_j	b_{j+1}	C_1	C_2	C_3	C_4	h	RMS
0.35	0.7	1.32467	-0.0413302	0.0394627	-0.0160722	0.35	1.03E-04

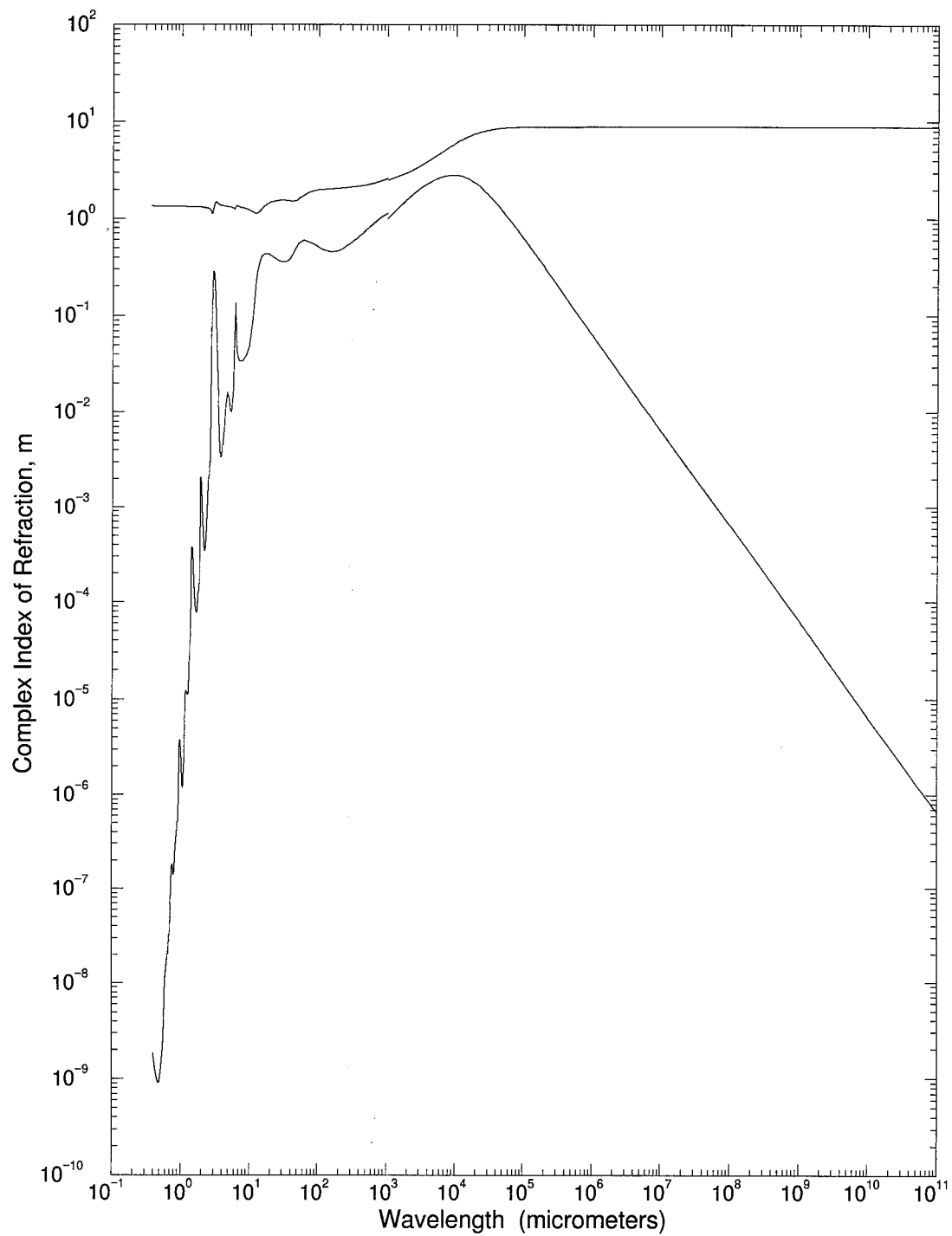


Figure 3.11. Complex indices of refraction for water over entire spectrum in this study. — Fitted n (top) and k (bottom) at 25°C.

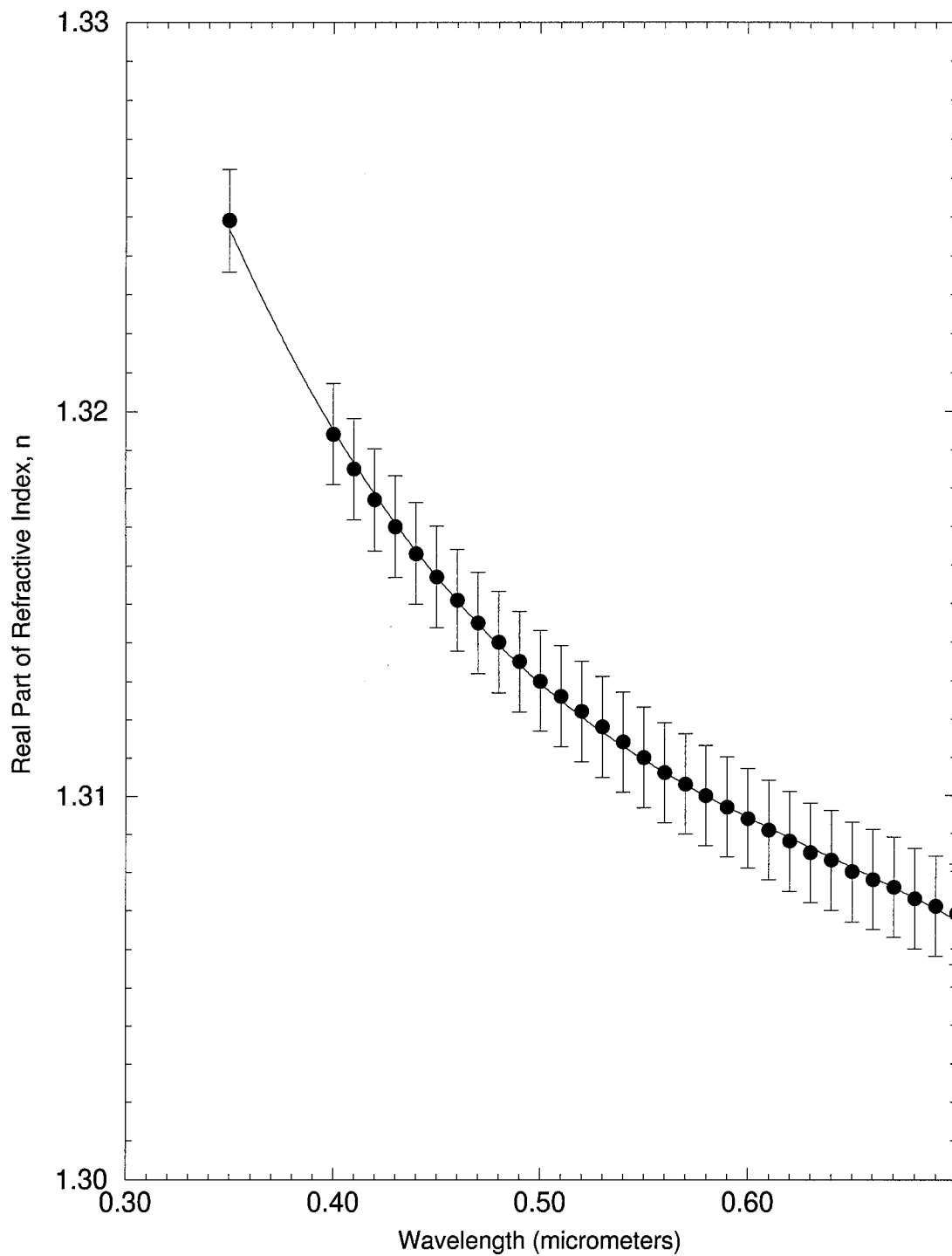


Figure 3.12. Real part of the complex index of refraction for ice in the visible region. — Fitted Curve; • Warren [1984] at -7°C , uncertainty of $\pm 0.1\%$.

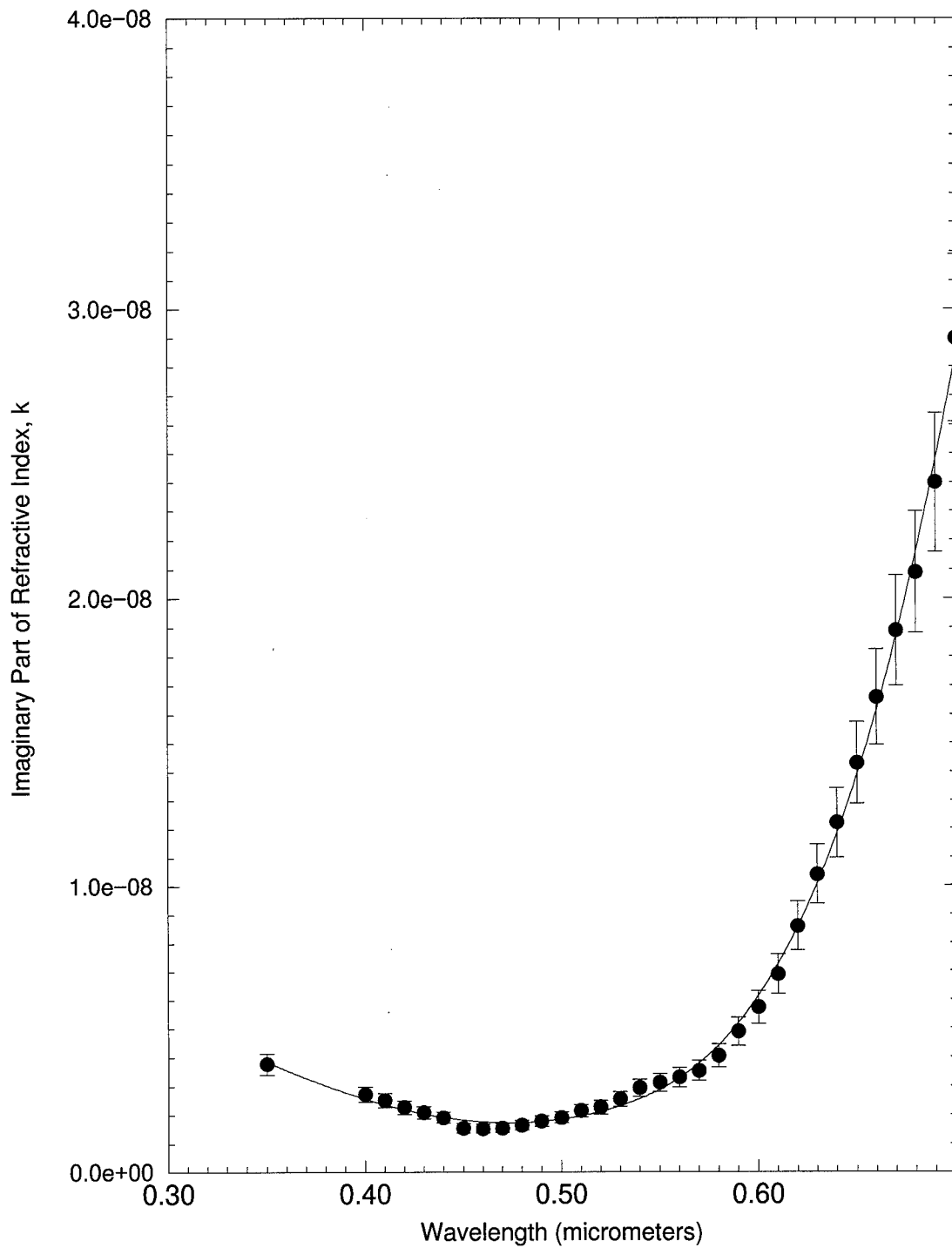


Figure 3.13. Imaginary part of the complex index of refraction for ice in the visible region. — Fitted Curve; • Warren [1984] at -7°C , uncertainty of $\pm 10\%$.

Table 3.10. Coefficient data of ice in the visible for k.

b_j	b_{j+1}	C_1	C_2	C_3	C_4	h	RMS
0.350	0.525	3.84987E-09	-5.28685E-09	2.25940E-09	1.38411E-09	0.175	3.53E-10
0.525	0.700	2.20653E-09	3.38428E-09	6.41173E-09	1.63665E-08	0.175	

Near Infrared

The first segment fit for the real part in the near infrared uses Warren's data. The remaining three segments were fit with Warren, as well as Schaaf and Williams [1973]. Both data sets were equally weighted due to the same uncertainty. From these four segments, a total of seven splines were used. The coefficients are given in Table 3.11.

As can be seen in Figure 3.14, the near infrared region contains a significant fundamental for ice. From Hobbs

Table 3.11. Coefficient data of ice in the near infrared for n.

b_j	b_{j+1}	C_1	C_2	C_3	C_4	h	RMS
0.70000	1.98000	1.306890	-0.0262032	0.017956	-0.0240796	1.2800	1.52E-04
1.98000	2.44750	1.275250	-0.0261000	-0.001490	-0.0128000	0.4675	3.56E-03
2.44750	2.91500	1.234880	-0.0674000	-0.039800	-0.1845630	0.4675	
2.91500	3.00833	0.946601	0.2862440	-0.480584	0.2914220	0.0933	1.05E-02
3.00833	3.10167	1.043680	0.1993420	0.393682	-0.1962340	0.0933	
3.10167	3.19500	1.440470	0.3980040	-0.195020	0.0082700	0.0933	
3.19500	4.00000	1.663530	-0.7989280	0.764544	-0.2668760	0.8050	3.69E-03

[1974], a wavenumber of 3300 cm^{-1} , or $3.03 \text{ }\mu\text{m}$, corresponds to the O-H stretching fundamental, or ν_1 .

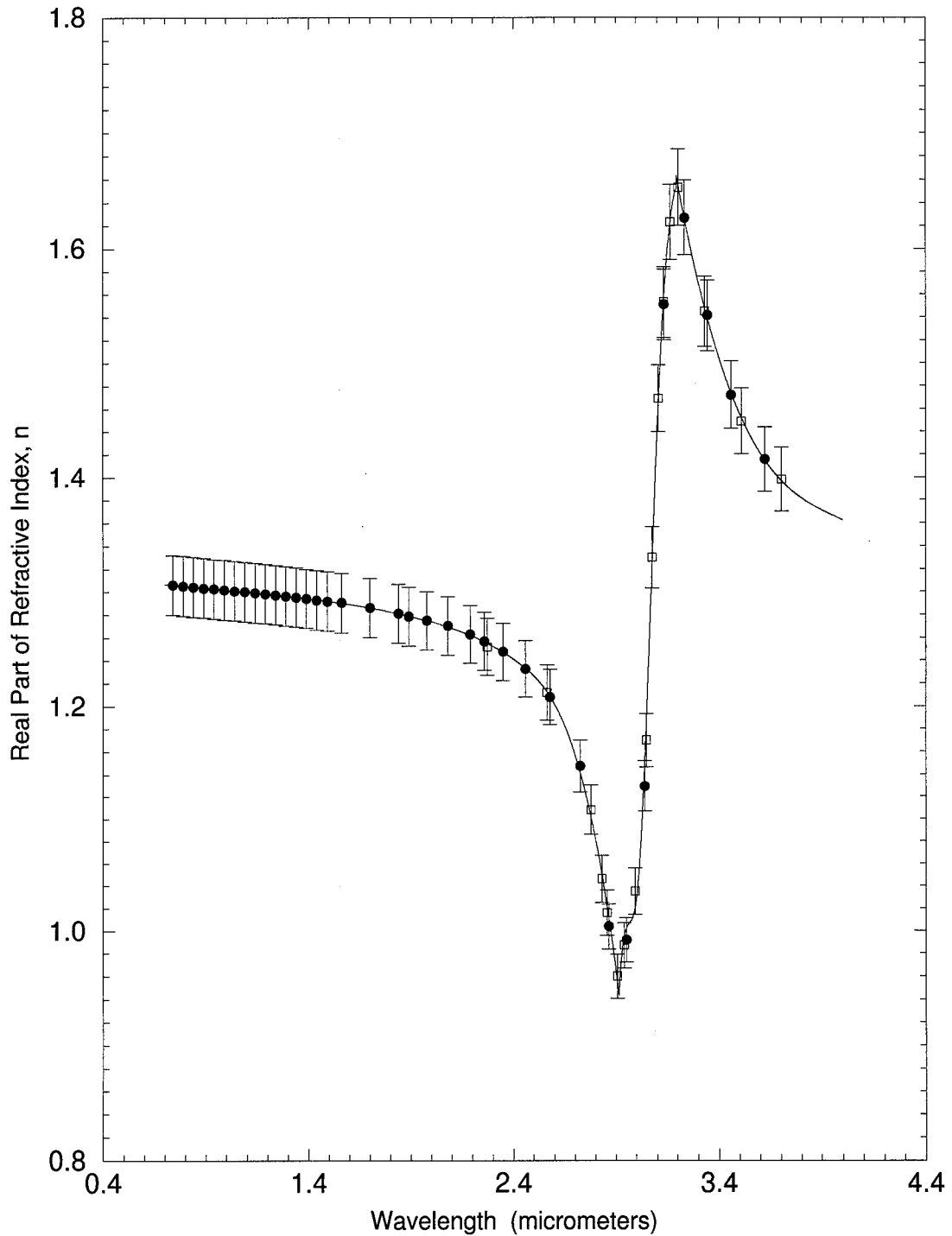


Figure 3.14. Real part of the complex index of refraction for ice in the near infrared region. — Fitted Curve; • Warren [1984] at -7°C , uncertainty of $\pm 2\%$; □ Schaaf and Williams [1973] at -7°C , uncertainty of $\pm 2\%$.

An additional feature to note is the drop of n below 1.0 within the dispersion region. To many, this would be a blatant violation of relativity, as electromagnetic energy is apparently traveling faster than the speed of light. This is not the case. By definition, the real part determines phase velocity

$$u_p = \frac{c}{n}. \quad 3.3$$

Invoking an n less than 1.0 would mean a violation of the theory of relativity. This is only true for material objects or signals. Phase is neither of these. The speed at which a signal travels through a medium is not measured by how fast the peak to peak phase propagates, but rather how fast the signal reaches a receptor in a known distance.

Bohren and Huffman [1983] present two case examples as to why n deviates from 1.0. The one of interest is when n is less than 1.0.

Given a slab of oscillators, in this study these will be the H_2O molecules, and an incident wave propagating through the slab at steady state, the reaction of the oscillators to the incident wave produces scattering. The direction of interest will be the scattered wave along the incident wave. This scattered wave combines with the incident wave. From the Lorentz model, the incident wave and oscillator can have a relative phase difference of 0° to

180°. Bohren and Huffman have shown that the scattered wave will be 90° out of phase to the relative phase at the resonant frequency. At the resonant frequency, the combined scattered and incident wave, or transmitted wave, are in phase producing the maximum amplitude. Above the resonant frequency, the scattered wave begins to lead the incident wave producing a transmitted wave with a phase ahead of the incident wave. This phase lead gives the impression that the signal has accelerated faster than the speed of light within the slab, while, in reality, no laws of physics have been violated.

The imaginary part in the near infrared is just as complex as that in water. This region required 11 segments with a total of 33 splines. The coefficients for these splines are given in Table 3.12. The use of this many splines preserved every absorption band. Warren's data were used throughout this region. Kou et al. [1993] provided data from 1.45 μm to 2.5 μm . Within this region, Kou et al.'s data received the majority of the weighting due to the low uncertainty of 1 to 2 percent. This weighting comprised of 0.7. Beyond 2.5 μm , Schaaf and Williams [1973] and Warren's data were combined equally.

Table 3.12. Coefficient data of ice in the near infrared for k.

b_j	b_{j+1}	C_1	C_2	C_3	C_4	h	RMS
0.70000	0.77750	2.8637E-08	3.2534E-08	3.4804E-08	-5.4400E-09	0.077500	2.71E-08
0.77750	0.85500	9.0535E-08	8.5822E-08	1.8484E-08	2.8047E-08	0.077500	
0.85500	0.93250	2.2289E-07	2.0693E-07	1.0263E-07	1.3790E-08	0.077500	
0.93250	1.01000	5.4624E-07	4.5355E-07	1.4400E-07	8.6964E-07	0.077500	
1.01000	1.15000	1.8100E-06	6.5300E-06	-1.9900E-05	1.4000E-05	0.140000	3.18E-07
1.15000	1.29000	2.4400E-06	8.7200E-06	2.2100E-05	-2.0000E-05	0.140000	
1.29000	1.34000	1.3200E-05	-7.0300E-07	1.0600E-06	-1.1300E-07	0.050000	9.67E-08
1.34000	1.39000	1.3500E-05	1.0900E-06	7.2600E-07	2.0600E-06	0.050000	
1.39000	1.44150	1.5500E-05	-6.5600E-06	1.2100E-04	3.4400E-05	0.051500	2.94E-05
1.44150	1.49300	1.6400E-04	3.3900E-04	2.2400E-04	-1.6100E-04	0.051500	
1.49300	1.60525	5.7300E-04	-2.1400E-04	-2.2100E-04	1.4200E-04	0.112250	2.45E-05
1.60525	1.71750	2.8000E-04	-2.3100E-04	2.0400E-04	-8.3400E-05	0.112250	
1.71750	1.82975	1.6900E-04	-7.4400E-05	-4.6500E-05	5.8900E-05	0.112250	
1.82975	1.94200	1.0700E-04	9.3200E-06	1.3000E-04	8.3500E-04	0.112250	
1.94200	2.09600	1.0500E-03	3.5100E-03	-5.9800E-03	2.3000E-03	0.154000	3.09E-05
2.09600	2.25000	8.7600E-04	-1.5600E-03	9.0800E-04	6.8700E-07	0.154000	
2.25000	2.32400	2.0900E-04	-2.1600E-05	3.2500E-04	-1.1500E-04	0.074000	4.22E-05
2.32400	2.39800	3.9800E-04	2.8400E-04	-1.9500E-05	-2.8500E-05	0.074000	
2.39800	2.47200	6.3400E-04	1.6000E-04	-1.0500E-04	7.5100E-05	0.074000	
2.47200	2.54600	7.6400E-04	1.7600E-04	1.2100E-04	-1.5700E-04	0.074000	
2.54600	2.62000	9.0300E-04	-5.4500E-05	-3.5100E-04	8.5400E-04	0.074000	
2.62000	2.77650	1.1100E-03	1.7400E-02	-3.5300E-02	3.4600E-02	0.156500	2.94E-03
2.77650	2.93300	1.7900E-02	5.0800E-02	6.8600E-02	1.4248E-01	0.156500	
2.93300	2.97740	2.7716E-01	8.7000E-02	7.6600E-03	-8.8700E-05	0.044400	2.77E-03
2.97740	3.02180	3.7175E-01	1.0200E-01	7.3900E-03	1.2400E-02	0.044400	
3.02180	3.06620	4.9357E-01	1.5391E-01	4.4400E-02	-6.8800E-02	0.044400	
3.06620	3.11060	6.2314E-01	3.6400E-02	-1.6191E-01	5.6000E-02	0.044400	
3.11060	3.15500	5.5362E-01	-1.1952E-01	5.9500E-03	-1.3500E-03	0.044400	
3.15500	3.22750	4.3970E-01	-2.5022E-01	-2.5900E-02	4.4300E-02	0.072500	3.39E-03
3.22750	3.30000	2.0794E-01	-1.6899E-01	1.0710E-01	-4.4500E-02	0.072500	
3.30000	3.53333	1.0200E-01	-2.1696E-01	1.8272E-01	-5.5400E-02	0.233333	5.91E-04
3.53333	3.76667	1.2700E-02	-1.7600E-02	1.6600E-02	-5.0600E-03	0.233333	
3.76667	4.00000	6.6500E-03	4.5200E-04	1.4500E-03	1.4800E-03	0.233333	

Looking at Figure 3.15, three significant bands appear in this region. The strongest absorption band is the O-H stretching fundamental previously discussed. The other two bands are combinational modes made possible by the disordered lattice of ice. Johari [1981] describes these

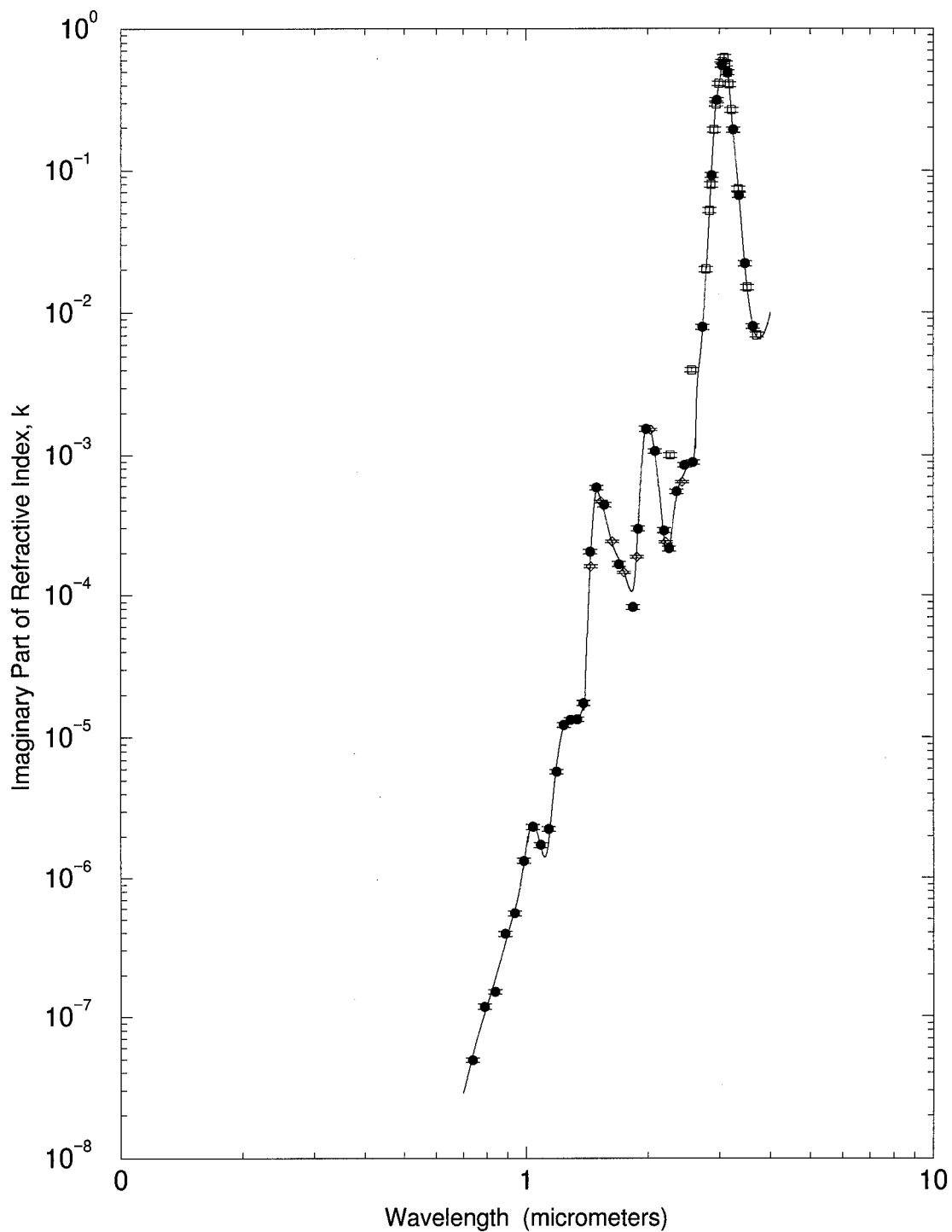


Figure 3.15. Imaginary part of the complex index of refraction for ice in the near infrared region. — Fitted Curve; • Warren [1984] at -7°C , uncertainty of $\pm 4\%$; □ Schaaf and Williams [1973] at -7°C , uncertainty of $\pm 4\%$; ◇ Kou et al. [1993] at -25°C , uncertainty of $\pm 2\%$.

modes as combinations and overtones of hindered translation, ν_T , rotation, ν_R , or the ν_2 fundamental associated with bending.

Middle Infrared

The middle infrared region for the real and imaginary parts of the refractive index was fit with Warren, and Schaaf and Williams' data with equal weighting, again due to their same uncertainty. The real part consisted of 8 segments with 26 splines, and the imaginary part had 10 segments with 30 splines. As can be seen from the number of splines, both parts have complex shapes in this region. Tables 3.13 and 3.14 contain the coefficients for n and k , respectively.

From Figures 3.16 and 3.17, five major features can be identified. From Figure 3.17, four absorption bands exist in the middle infrared. At 2200 cm^{-1} ($4.55 \text{ }\mu\text{m}$) there is a combination band consisting of the ν_2 and ν_L fundamentals. Further into the middle infrared band, a ν_2 fundamental peaks around $6.14 \text{ }\mu\text{m}$. The next band is at $12.2 \text{ }\mu\text{m}$. This absorption region corresponds to the ν_L fundamental. The last absorption band at around $49 \text{ }\mu\text{m}$, is due to hindered translation. The continuum region of 8.5 to $12.5 \text{ }\mu\text{m}$ is as

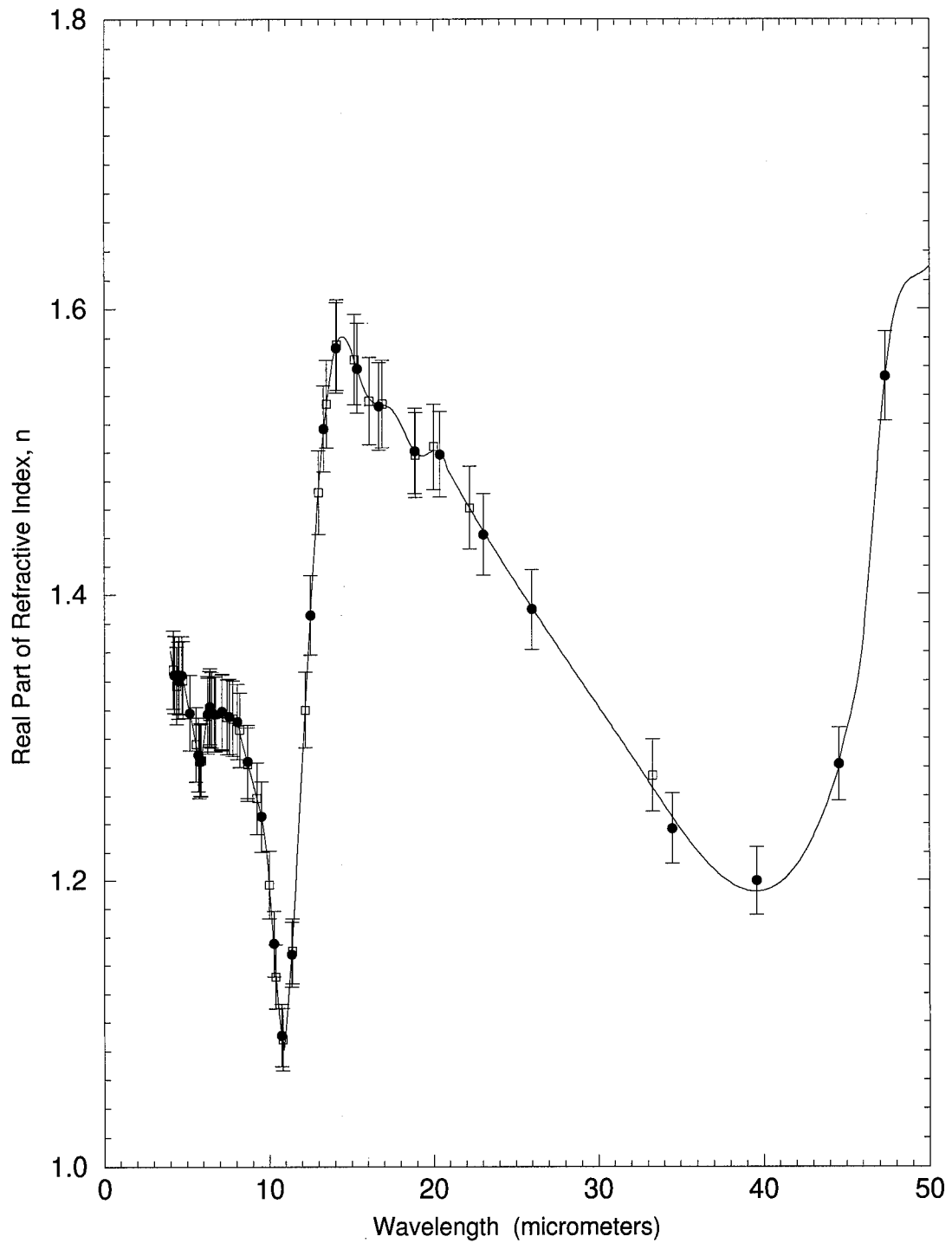


Figure 3.16. Real part of the complex index of refraction for ice in the middle infrared region. — Fitted Curve; • Warren [1984] at -7°C , uncertainty of $\pm 2\%$; □ Schaaf and Williams [1973] at -7°C , uncertainty of $\pm 2\%$.

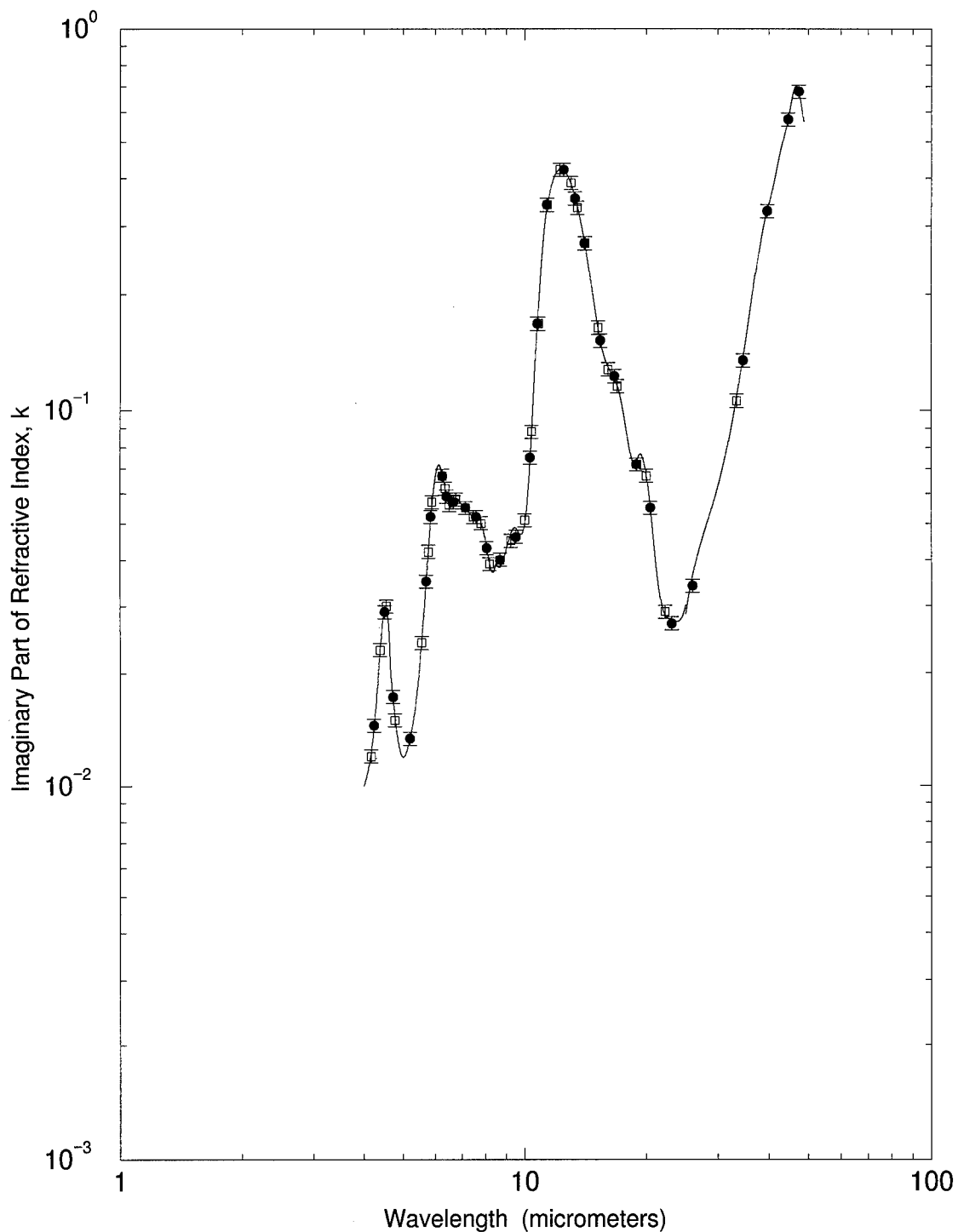


Figure 3.17. Imaginary part of the complex index of refraction for ice in the middle infrared region. — Fitted Curve; • Warren [1984] at -7°C , uncertainty of $\pm 4\%$; □ Schaaf and Williams [1973] at -7°C , uncertainty of $\pm 4\%$.

prominent a feature for ice as it is for water. A major difference exists, however. The ν_2 fundamental peaks at 12.2 μm and extends close to 10 μm . The continuum, in essence, abates for ice. Schaaf and Williams presented a table containing a compilation of fundamental data of different temperatures. As the temperature gets colder, the ν_L fundamental encroaches further into the continuum.

Table 3.13. Coefficient data of ice in the middle infrared for n.

b_j	b_{j+1}	C_1	C_2	C_3	C_4	h	RMS
4.00000	4.20267	1.36106	-0.016146	0.002456	-0.000908	0.202667	6.65E-04
4.20267	4.40533	1.34646	-0.013955	-0.000266	0.005173	0.202667	
4.40533	4.60800	1.33741	0.001032	0.015254	-0.006304	0.202667	
4.60800	5.02133	1.34747	-0.009420	-0.017900	0.007150	0.413333	6.06E-04
5.02133	5.43467	1.32728	-0.023800	0.003540	-0.002930	0.413333	
5.43467	5.84800	1.30408	-0.025500	-0.005260	0.010500	0.413333	
5.84800	6.25750	1.28438	0.020000	0.037800	-0.024700	0.409500	5.43E-04
6.25750	6.66700	1.31752	0.021500	-0.036300	0.013000	0.409500	
6.66700	7.17700	1.31615	0.008240	-0.006310	0.000487	0.510000	3.72E-04
7.17700	7.68700	1.31856	-0.002930	-0.004850	0.003750	0.510000	
7.68700	8.19700	1.31453	-0.001370	0.006410	-0.013300	0.510000	
8.19700	9.09800	1.30564	-0.042700	0.001650	0.000742	0.901000	3.49E-03
9.09800	9.99900	1.26529	-0.037200	0.003870	-0.032300	0.901000	
9.99900	10.90000	1.19963	-0.126433	-0.093100	0.105271	0.901000	
10.90000	12.55000	1.08067	0.177349	0.272327	-0.134574	1.650000	2.54E-03
12.55000	14.20000	1.39577	0.318282	-0.131394	-0.004850	1.650000	
14.20000	15.85000	1.57781	0.040900	-0.145938	0.070000	1.650000	
15.85000	17.50000	1.54280	-0.041000	0.064000	-0.036100	1.650000	
17.50000	19.15000	1.52973	-0.021200	-0.044200	0.033600	1.650000	
19.15000	20.80000	1.49792	-0.008860	0.056500	-0.054000	1.650000	
20.80000	32.69000	1.48981	-0.253114	0.074900	-0.035400	11.890000	5.17E-03
32.69000	44.58000	1.27625	-0.209394	-0.031200	0.244759	11.890000	
44.58000	45.94250	1.28179	0.094800	-0.088000	0.073000	1.362500	1.16E-03
45.94250	47.30500	1.36157	0.137783	0.131025	-0.082000	1.362500	
47.30500	48.66750	1.54836	0.153797	-0.115012	0.031200	1.362500	
48.66750	50.03000	1.61835	0.017400	-0.021400	0.015800	1.362500	

Table 3.14. Coefficient data of ice in the middle infrared for k.

b_j	b_{j+1}	C_1	C_2	C_3	C_4	h	RMS
4.00000	4.32550	0.009994	0.003234	-0.001186	0.006532	0.32550	5.49E-04
4.32550	4.65100	0.018575	0.020459	0.018411	-0.036744	0.32550	
4.65100	5.18400	0.020700	-0.030400	0.032000	-0.009110	0.53300	1.18E-03
5.18400	5.71700	0.013200	0.006260	0.004680	0.012000	0.53300	
5.71700	6.25000	0.036100	0.051700	0.040800	-0.062500	0.53300	
6.25000	6.51033	0.066900	-0.007820	-0.013200	0.009720	0.26033	5.45E-04
6.51033	6.77067	0.055600	-0.005160	0.015900	-0.008200	0.26033	
6.77067	7.03100	0.058100	0.002030	-0.008710	0.003960	0.26033	
7.03100	7.29133	0.055400	-0.003500	0.003180	-0.001650	0.26033	
7.29133	7.55167	0.053400	-0.002110	-0.001780	0.002100	0.26033	
7.55167	7.81200	0.051600	0.000609	0.004500	-0.006740	0.26033	
7.81200	8.47500	0.050000	-0.010200	-0.034600	0.033800	0.66300	6.51E-05
8.47500	9.45000	0.039900	-0.021000	0.068200	-0.038500	0.97500	5.40E-03
9.45000	10.42500	0.048700	-0.000022	-0.047200	0.089500	0.97500	
10.42500	11.40000	0.090900	0.173955	0.221168	-0.138669	0.97500	
11.40000	13.26750	0.341636	0.375274	-0.493724	0.139438	1.86750	2.10E-03
13.26750	15.13500	0.362624	-0.193859	-0.075400	0.072700	1.86750	
15.13500	17.00250	0.166048	-0.126603	0.142664	-0.067500	1.86750	
17.00250	18.87000	0.114613	-0.043800	-0.059800	0.061300	1.86750	
18.87000	20.91330	0.071600	0.051300	-0.144245	0.063900	2.04333	6.27E-04
20.91330	22.95670	0.042500	-0.045600	0.047400	-0.016700	2.04333	
22.95670	25.00000	0.027700	-0.000785	-0.002610	0.005940	2.04333	
25.00000	37.00000	0.028600	0.105864	-0.160120	0.250438	12.00000	3.01E-03
37.00000	39.75000	0.222941	0.128098	-0.033100	0.015200	2.75000	8.07E-03
39.75000	42.50000	0.333095	0.107386	0.012400	0.003200	2.75000	
42.50000	45.25000	0.456085	0.141791	0.022000	0.002860	2.75000	
45.25000	48.00000	0.622739	0.194379	0.030600	-0.225490	2.75000	
48.00000	49.01500	0.624998	-0.164523	0.152982	-0.052400	1.01500	1.40E-04
49.01500	50.03000	0.561033	-0.015800	-0.004290	0.002290	1.01500	

Far Infrared

Warren's data set was used to fit both the real and imaginary parts. A problem that exists in this region extends into the longwave spectrum. Past 200 μm , k becomes dependent on temperature. To a lesser extent, n does also. Physical equations do not accurately model ice in this region. This may also be in part due to the low amount, and

segmented nature, of data in this region. Warren presents data from temperatures of -1, -5, -20 and -60°C. No relationships are apparent between these sets. Since the dependence begins at a different wavelength for each temperature, the problem becomes even more complicated. However, as temperature decreases, so does k , and, to a lesser extent, so does n .

The odd behavior in this region appears to be related to the disparity of the data. Warren used optical constant data from five different authors. From these five authors, five different methodologies were used to produce five different results. A consistent experiment to measure the optical properties in this region should be done so that this region could be better modeled.

The -20°C temperature data were used for the fits in Figures 3.18 and 3.19, as this temperature is the closest average of the range presented. A temperature dependent coefficient was attempted, but was inconsistent with other measurements, and will not be presented to prevent the misconception of an accurate temperature-dependent model. The largest deviation between -1°C and -60°C for the real data is 0.6 percent. This value is smaller than many measurement uncertainties, therefore -20°C is a good

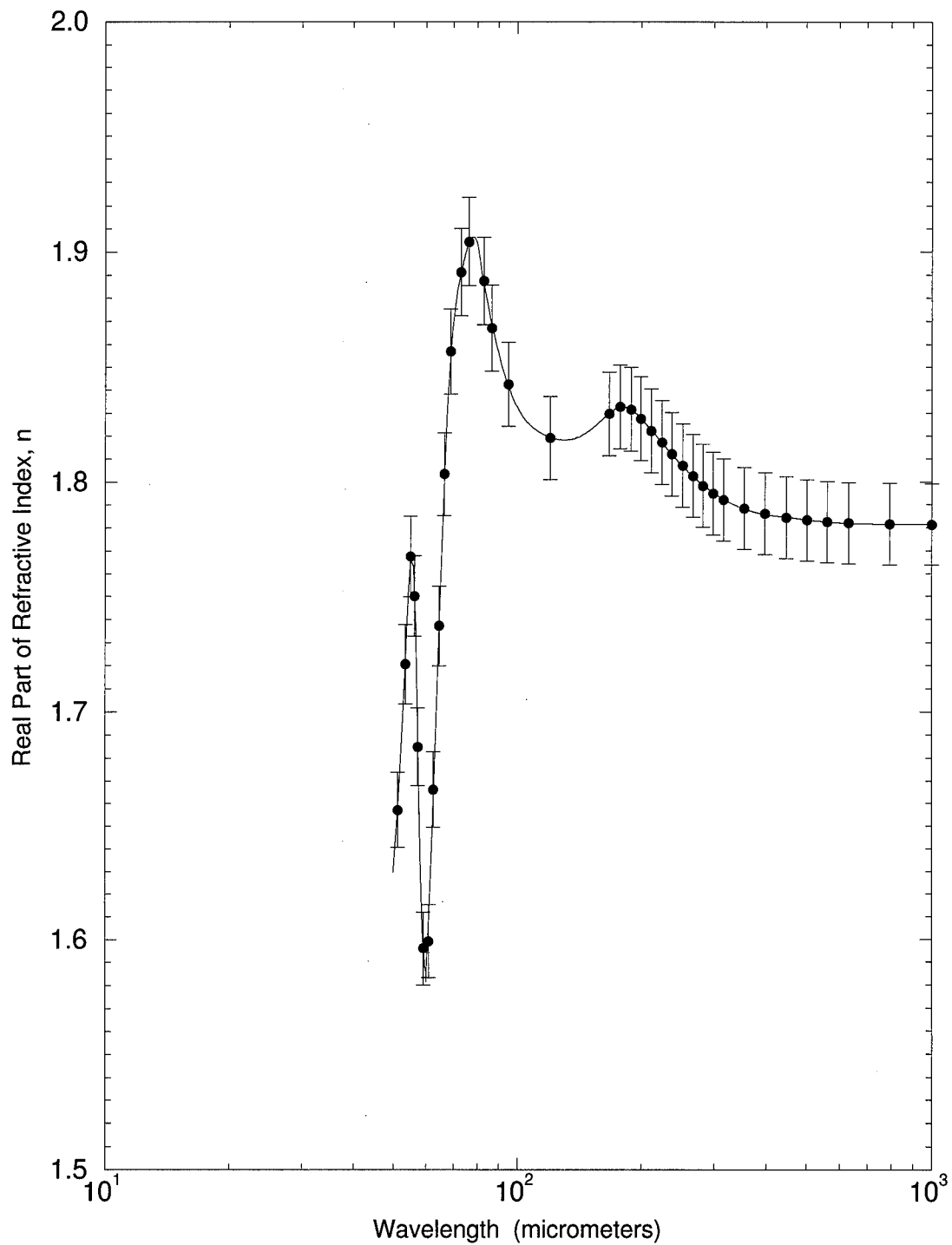


Figure 3.18. Real part of the complex index of refraction for ice in the far infrared region. — Fitted Curve; • Warren [1984] at -7°C , uncertainty of $\pm 1\%$.

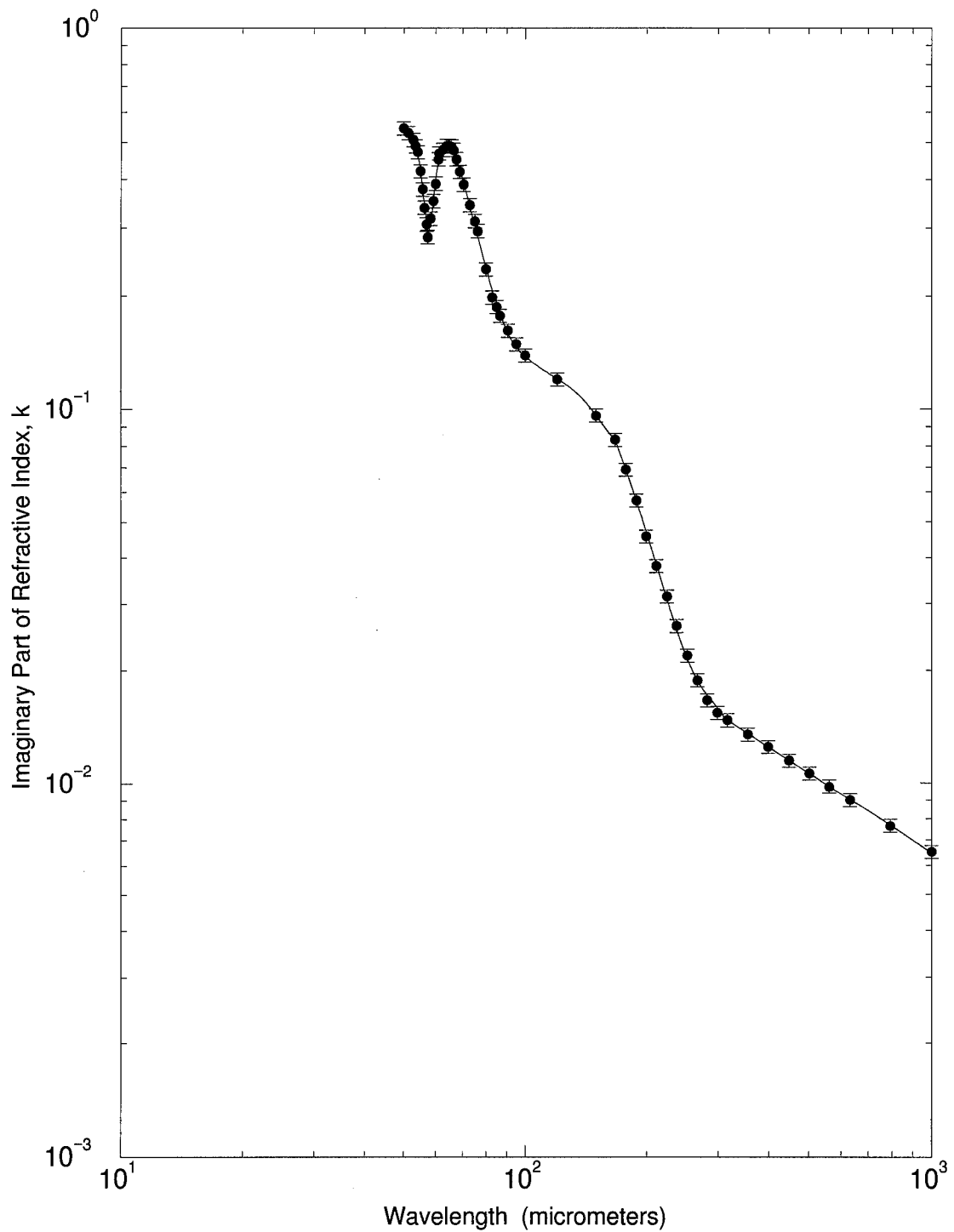


Figure 3.19. Imaginary part of the complex index of refraction for ice in the far infrared region. — Fitted Curve; • Warren [1984] at -7°C and -20°C , uncertainty of $\pm 4\%$.

baseline to fit. The coefficients for the fits of n and k are contained in Tables 3.15 and 3.16, respectively.

Table 3.15. Coefficient data of ice in the far infrared for n .

b_j	b_{j+1}	C_1	C_2	C_3	C_4	h	RMS
50.0300	51.6917	1.62960	0.030373	0.009752	-0.002008	1.66167	3.01E-03
51.6917	53.3533	1.66772	0.043854	0.003728	0.001802	1.66167	
53.3533	55.0150	1.71710	0.056715	0.009134	-0.017038	1.66167	
55.0150	56.6767	1.76591	0.023870	-0.041979	-0.009225	1.66167	
56.6767	58.3383	1.73858	-0.087762	-0.069653	0.046478	1.66167	
58.3383	60.0000	1.62764	-0.087635	0.069781	-0.024633	1.66167	
60.0000	66.6667	1.58159	0.145771	0.194599	-0.115299	6.66667	4.54E-03
66.6667	73.3333	1.80666	0.189072	-0.151297	0.048200	6.66667	
73.3333	80.0000	1.89261	0.031000	-0.006770	-0.013500	6.66667	
80.0000	112.8250	1.90317	-0.203132	0.175626	-0.053900	32.82500	8.71E-04
112.8250	145.6500	1.82172	-0.013700	0.013800	-0.000938	32.82500	
145.6500	178.4750	1.82086	0.011100	0.011000	-0.010400	32.82500	
178.4750	211.3000	1.83252	0.001890	-0.020100	0.007910	32.82500	
211.3000	356.2500	1.82259	-0.068800	0.044900	-0.010700	144.95000	3.19E-04
356.2500	501.2000	1.78803	-0.011000	0.012900	-0.006780	144.95000	
501.2000	1000.0000	1.78320	-0.006840	0.009820	-0.004780	498.80000	1.41E-07

Microwave/Radiowave

Warren's data were used for the fit of k only as shown in Figure 3.20. The imaginary part is highly temperature dependent in this region. As was stated in the previous section, no physical equations exist to model this region. Warren's -20°C data were used to fit k . The real part was computed using the Wörz-Cole equations, 2.26 and 2.27. Though these equations are valid only in the longwave, good approximations can be made in the microwave/radiowave

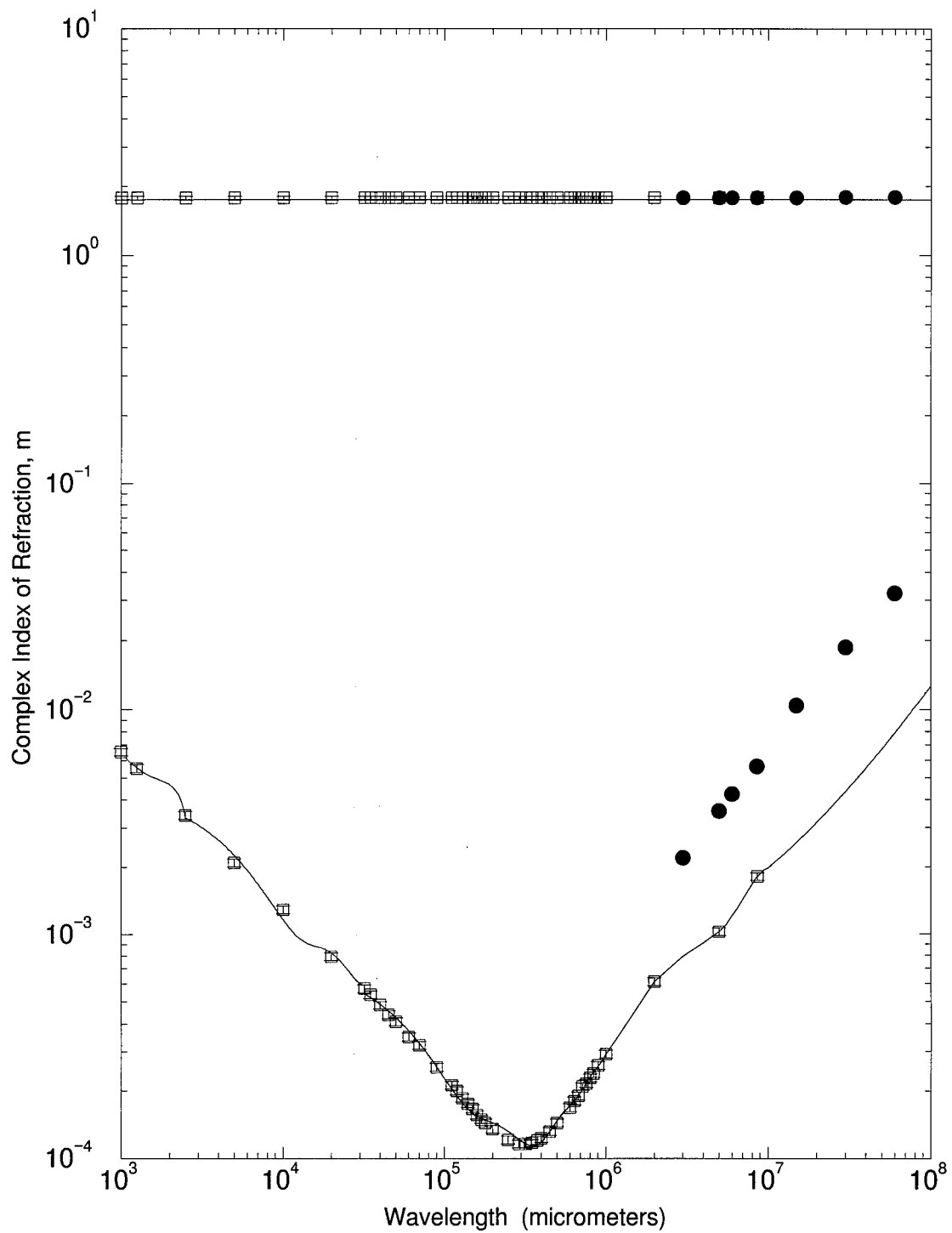


Figure 3.20. Complex indices of refraction for ice in the microwave/radiowave region. — Calculated n (top) and fitted k (bottom); • Johari [1976] at -5°C , uncertainty of $\pm 0.3\%$ for n and $\pm 2\%$ for k ; □ Warren [1984] at -20°C , uncertainty of $\pm 1\%$ for n and $\pm 4\%$ for k .

region, as well. Johari's [1976] data were plotted to show the temperature dependence in this region. His values were measured at -5°C . The coefficients for k are given in Tables 3.16 and 3.17.

Table 3.16. Coefficient data of ice in the far infrared and into the microwave for k .

b_j	b_{j+1}	C_1	C_2	C_3	C_4	h	RMS
50.0300	53.7450	0.543650	-0.077605	0.111533	-0.093882	3.7150	4.57E-03
53.7450	57.4600	0.483696	-0.136185	-0.170112	0.106584	3.7150	
57.4600	60.3450	0.286554	-0.008900	0.269159	-0.126978	2.8850	7.91E-03
60.3450	63.2300	0.419840	0.148488	-0.111775	0.031100	2.8850	
63.2300	66.1150	0.487667	0.018300	-0.018400	-0.006700	2.8850	
66.1150	69.0000	0.480818	-0.038700	-0.038500	0.015100	2.8850	
69.0000	101.6667	0.424095	-0.768335	0.709198	-0.228879	32.6667	5.59E-03
101.6667	134.3330	0.136079	-0.036600	0.022600	-0.011700	32.6667	
134.3330	167.0000	0.110414	-0.026400	-0.012400	0.011400	32.6667	
167.0000	316.2000	0.082900	-0.212885	0.236667	-0.092400	149.2000	6.11E-04
316.2000	562.3000	0.014700	-0.008000	0.004510	-0.001420	246.1000	3.61E-05
562.3000	2500.0000	0.009740	-0.020600	0.030800	-0.016600	1937.7000	5.31E-05

Table 3.17. Coefficient data of ice in the microwave and into the longwave for k .

b_j	b_{j+1}	C_1	C_2	C_3	C_4	h	RMS
2.500E+03	1.725E+04	3.337E-03	-7.553E-03	7.874E-03	-2.791E-03	1.475E+04	7.01E-05
1.725E+04	3.200E+04	8.682E-04	-1.766E-04	-4.982E-04	3.969E-04	1.475E+04	
3.200E+04	1.933E+05	5.410E-04	-1.160E-03	1.170E-03	-4.010E-04	1.613E+05	1.10E-05
1.933E+05	3.547E+05	1.450E-04	-3.020E-05	-3.500E-05	3.370E-05	1.613E+05	
3.547E+05	5.160E+05	1.140E-04	8.260E-07	6.600E-05	-2.900E-05	1.613E+05	
5.160E+05	6.773E+05	1.510E-04	4.590E-05	-2.100E-05	1.360E-05	1.613E+05	
6.773E+05	8.387E+05	1.900E-04	4.470E-05	1.980E-05	-1.240E-05	1.613E+05	
8.387E+05	1.000E+06	2.420E-04	4.720E-05	-1.730E-05	2.000E-05	1.613E+05	
1.000E+06	5.500E+06	2.920E-04	1.830E-03	-2.030E-03	1.000E-03	4.500E+06	0.0
5.500E+06	1.000E+07	1.100E-03	7.790E-04	9.800E-04	-8.790E-04	4.500E+06	
1.000E+07	1.500E+09	1.980E-03	1.762E-01	-8.340E-07	7.450E-08	1.500E+09	2.48E-07

Longwave

Figure 3.21 shows the plot for n and k for ice in the longwave region. Much of this region is plotted using the Wörz-Cole equations. The onset of the k data had to be fit with an extrapolation of Warren's data to the valid region of the Wörz-Cole equations, which is a wavelength of 1.5 km or $1.5 \times 10^9 \mu\text{m}$. The coefficients associated with this fit are found in Table 3.17. These plots are valid for a temperature of -20°C . Two additional plots were made at -5°C to compare with the data measured by Johari [1976]. There are discrepancies between the data and equations. These are probably due to parameterization uncertainties of τ , σ_0 , and ϵ_0 from the Wörz-Cole equations.

The broad absorption band is due to orientation polarization. Johari [1981] states that this region moves to longer wavelengths as temperature decreases. The Wörz-Cole equations produce this temperature transition.

Summary

A broadband picture for the refractive indices of ice for the spectrum discussed is presented in Figure 3.22. The valid temperature is -20°C

Uncertainty Incorporation

The models presented in this study are not without

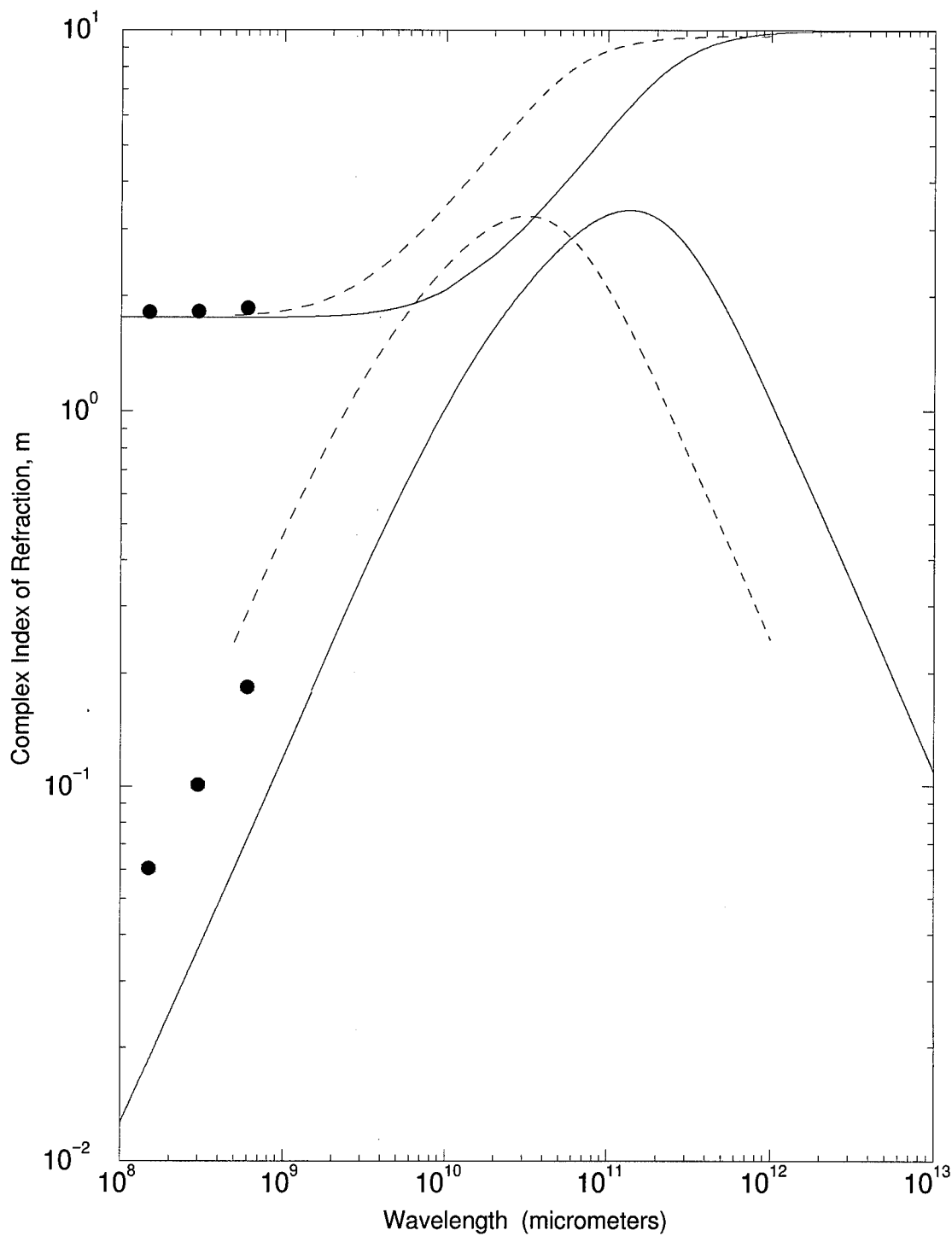


Figure 3.21. Complex indices of refraction for ice in the longwave region. — Calculated n (top) and k (bottom) at -20°C ; --- Calculated n (top) and k (bottom) at -5°C ; • Johari [1976] at -5°C , uncertainty of $\pm 0.3\%$ for n and $\pm 2\%$ for k .

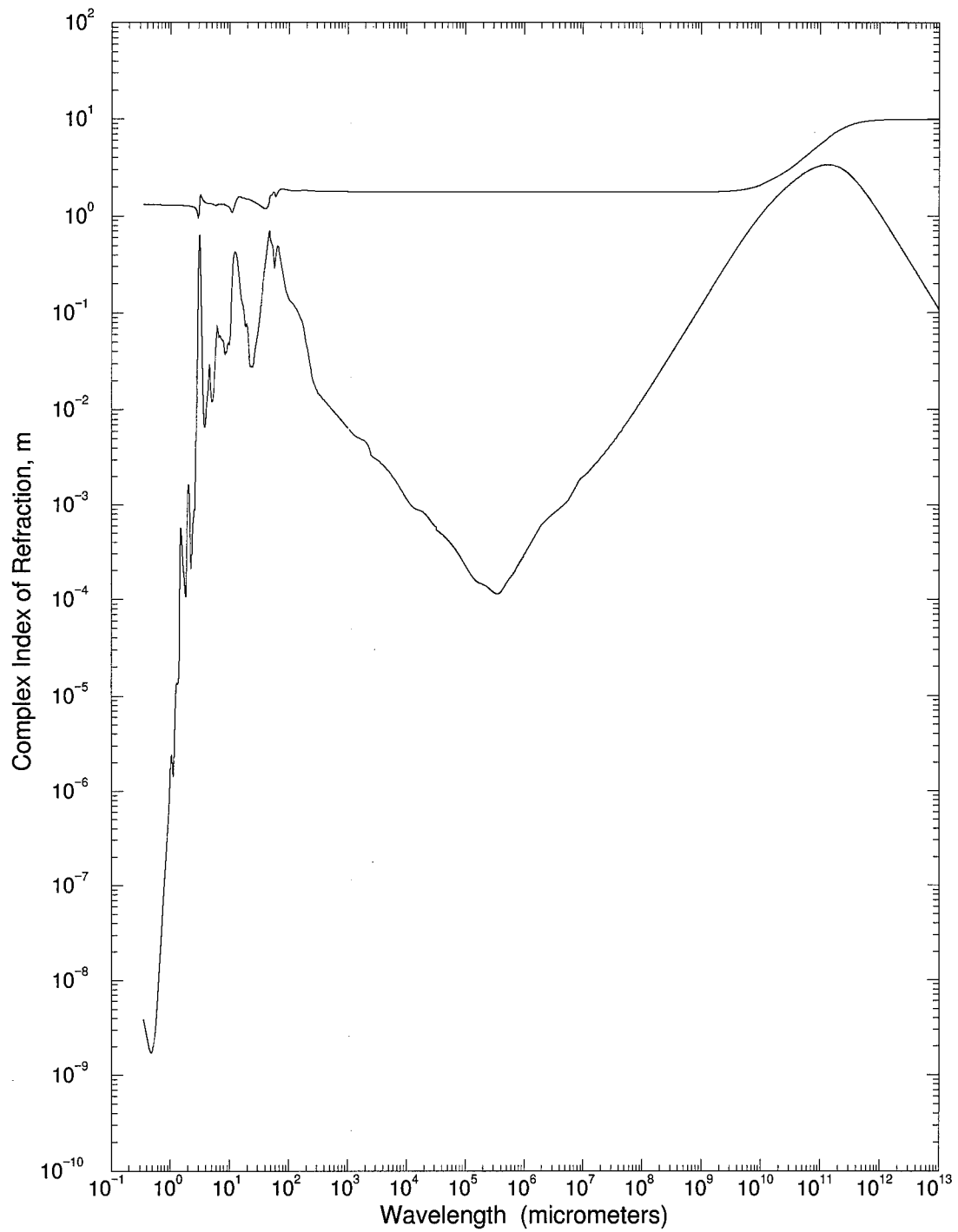


Figure 3.22. Complex indices of refraction for ice over entire spectrum in this study. — n (top) and k (bottom) at -20°C .

uncertainties. Each segment was visually inspected to ensure the behavior of each segment followed that of the data. Inspection of the RMS values of each segment provided shows the uncertainty of the fit is generally under 1 percent. A few segments, in particular, the far infrared k values for water, have higher values of the RMS. As was discussed, this was due to a high degree of variability in the data. Excluding this section, a conservative uncertainty associated with the fitting is ± 1 percent. The majority of the RMS values do show uncertainties well under this value and can be used if fitting is done on a smaller scale. If the k values for the far infrared region of water are used, an uncertainty of no less than ± 5 percent should be used for the model. The variability of the measurements precludes a more accurate model. Tables 3.18 and 3.19 provide the uncertainties for the combination of fit and data for water and ice, respectively. This should be the uncertainty incorporated when using fits for a particular region.

Table 3.18. Model uncertainties for water.

Optical Constant	Visible	Near Infrared	Middle Infrared	Far Infrared	Microwave Radiowave	Longwave
n	$\pm 0.0018\%$	$\pm 2.06\%$	$\pm 3.04\%$	$\pm 3.61\%$	$\pm 5.0\%$	$\pm 5.0\%$
k	$\pm 4.47\%$	$\pm 4.12\%$	$\pm 4.12\%$	$\pm 6.40\%$	$\pm 5.0\%$	$\pm 5.0\%$

Table 3.19. Model uncertainties for ice.

Optical Constant	Visible	Near Infrared	Middle Infrared	Far Infrared	Microwave Radiowave	Longwave
n	±0.10%	±2.24%	±2.24%	±1.12%	±5.0%	±5.0%
k	±10.05%	±4.47%	±4.47%	±4.12%	±4.12%	±5.0%

CHAPTER 4
CONCLUSIONS/FUTURE WORK

Methodology

For the technique used in this study, many interpolation schemes exist. The power of today's computers would allow a more accurate, complex interpolation scheme to be feasible in the sense of computational time; however, a low-order scheme with high accuracy fits was deemed as sufficient and realistic for incorporation into other work.

If equations existed to accurately explain the behavior of an E-M spectra, they were used in lieu of a fit, but not at the cost of accuracy. Though a powerful tool, the Kramers-Kronig relation could not be used to give an empirical formula describing the behavior of n and k as a function of wavelength. The equation requires an entire set of n or k data to compute the other and therefore, does not make sense to employ in this application. The Kramers-Kronig relation is primarily used to ensure proper behavior between n and k . This relation will not give a correct answer from its solution as it is dependent on a measured set of data. Incorrect measurements of k will result in

incorrect calculations of n . The use of this equation for a study such as this would be to ensure the behavior of the fitted curves in the dispersion regions is correct by comparing the calculation of the new data, n or k , with the data from the sources listed in Tables 1.1 or 1.2. I could also be used to see how uncertainty in the fitted curves of the absorption band propagates to the real part. The methodology used in this study is not and will not be the only one. Breakthroughs in spectral physics and computational methods could lead to even simpler behavioral models of the complex indices of refraction.

Data

Data measurements seem to have a high correlation to the advent of technology. For the infrared measurements, the dates correspond to the development of satellite technology. The problem that exists with past data sets and even those used in this study, is the high variability in temperature and spectral interval. The methods of data acquisition differ highly due to improvements in technology as well as the different means needed for long wavelengths versus the short wavelengths. An additional problem is the various sampling resolutions found in the data, many of which are low due to the technology constraints.

To ensure continuity, measurements should be taken for water and ice through much of the E-M spectrum using at least four atmospheric temperature constraints for both media in one experiment. This would validate or contradict physical equations such as Cole-Cole and Wörz-Cole, and provide a larger data base to create empirical formulae in the regions not described by such equations.

Authors compiling data should include not only tabulated data, but the criteria involved with measurement of the data. Uncertainty, temperature and pressure are all important to a study such as this. Some data in the compilations such as "private communications" cannot be obtained. It should be the responsibility of the author to ensure all parameters of the data collection are elaborated in their studies.

APPENDIX A
DESCRIPTION OF FUNDAMENTALS

Vibrational

The vibrational fundamentals, ν_1 and ν_3 , corresponds to the movement of the hydrogen molecules along the oxygen-hydrogen axis. Two kinds of movement are possible: symmetrical, ν_1 , and asymmetrical, ν_3 . Figure A.1 depicts these motions. The restoring force is dictated by the molecular distance between the H and O molecules. This distance ranges from 0.958 angstroms for liquid water to 1.011 angstroms in the ice lattice. These fundamentals are also referred to as translational fundamentals, or O-H stretching fundamental.

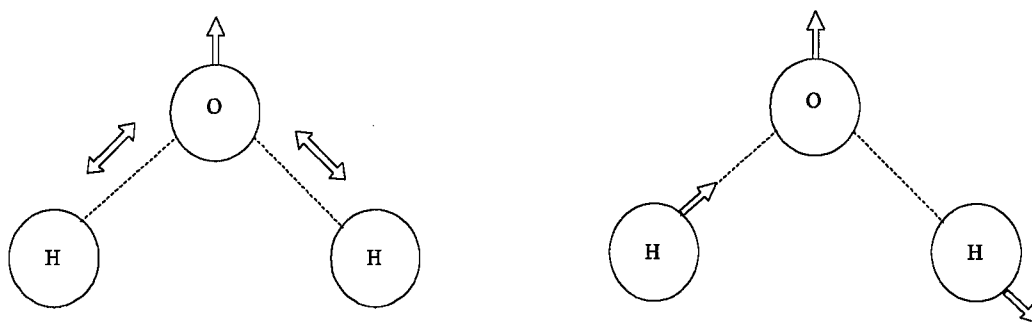


Figure A.1. Symmetrical stretching, ν_1 , (left) and asymmetrical stretching, ν_3 , (right).

Bending

The bending fundamental, ν_2 , corresponds to movement perpendicular to the O-H axis. Figure A.2 is a pictorial description of this motion. The restoring force is dictated by the angle between the two O-H axes, or 105° .

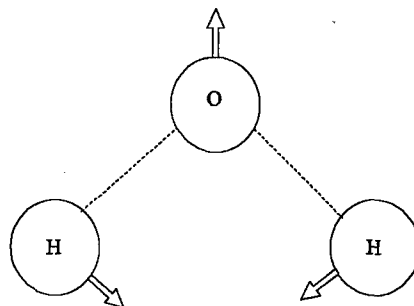


Figure A.2. Bending fundamental, ν_2 .

Rotational

The rotational, or librational fundamental is denoted by the symbol, ν_L . This fundamental is a rotation of the H₂O about the symmetrical axis as shown in Figure A.3. Since the molecule is not being deformed, there is no molecular restoration force. The cessation of librational spin is dictated by a relaxation time, or the amount of time needed for the molecule to return to a non-excited state. In essence, magnetism plays an important role for returning

the molecule to a lower state of excitation. Franks [1972] describes these mechanisms in detail.

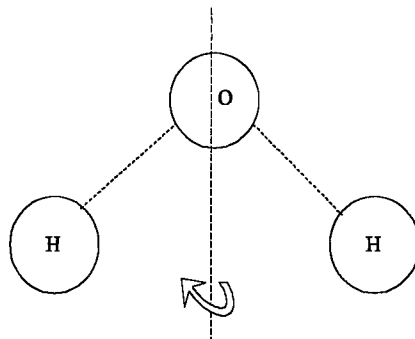


Figure A.3. Rotational, or Librational, fundamental, ν_L .

Hindered Translational

The hindered translational, ν_T , fundamental is associated with stretching of the hydrogen bond. Hasted [1973] describes this mode as a rigid, internal oscillation of the water molecule. This fundamental is depicted in Figure A.4. The restoration force is the distance maintained by the hydrogen bond. This distance varies in liquid water with angle of the bend in the hydrogen bond coupling. This distance variation is from 0.46 angstroms to 0.74 angstroms. Since ice is in a lattice form, the distance is maintained at 0.738 angstroms.

Orientation

The primary mechanism for the orientation fundamental

is lattice defects. Though prominent in ice, this fundamental also occurs in liquid water when hydrogen bonds become broken. During orientation, an H_2O molecule rotates through 120° about one of the hydrogen bonds. When this happens, two hydrogen atoms are left between two oxygen atoms ($O-H H-O$), as well as no hydrogen atoms between a pair of oxygen atoms ($O---O$). These two defects are called D and L defects, respectively, or Bjerrum defects. Reorientation of the water molecule occurs at these defects.

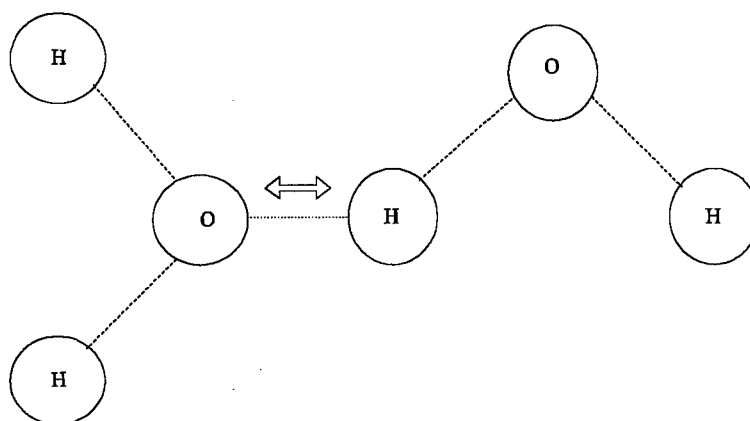


Figure A.4. Hindered translational fundamental, v_T .

REFERENCES

- Adler, R. F., H. Y. M. Yeh, N. Prasad, W. K. Tao and J. Simpson, 1991: Microwave simulations of a tropical rainfall system with a three-dimensional cloud model. *J. Appl. Meteor.*, **30**, 924-953.
- Afsar, M. N., and J. B. Hasted, 1977: Measurements of the optical constants of liquid H₂O and D₂O between 6 and 450 cm⁻¹. *J. Opt. Soc. Am.*, **67**, 902-904.
- Afsar, M. N., and J. B. Hasted, 1978: Submillimetre wave measurements of optical constants of water at various temperatures. *Infrared Phys.*, **18**, 835-841.
- Boguth, W., 1973: Refractive indices of liquids and solutions. *Micro. Acta.*, **74**, 217-221.
- Bohren, C. E., and D. R. Huffman, 1983: *Absorption and Scattering of Light by Small Particles*. Wiley and Sons, 530 pp.
- Cole, K. S., and R. H. Cole, 1941: Dispersion and absorption in dielectrics. *J. Chem. Phys.*, **9**, 341-351.
- Debye, P., 1929: *Polar Molecules*. Dover Publications, 172 pp.
- Downing, H. D., and D. Williams, 1975: Optical constants of water in the infrared. *J. Geophys. Res.*, **80**, 1656-1661.
- Franks, F., 1972: *Water: A Comprehensive Treatise Vol 1, The Physics and Physical Chemistry of Water*. Plenum Press, 596pp.
- Gough, S. R., 1972: A low temperature dielectric Cell and the permittivity of hexagonal ice to 2 K. *Can. J. Chem.*, **50**, 3046-3051.
- Grant, E. H., and R. J. Sheppard, 1974: Dielectric relaxation in water in the neighborhood of 4 °C. *J. Chem. Phys.*, **60**, 1792-1796.

- Grenfall, T. C., and D. K. Perovich, 1981: Radiation absorption coefficients of polycrystalline ice from 400-1400 nm. *J. Geophys. Res.*, **86**, 7447-7450.
- Hale, G. M., and M. R. Querry, 1973: Optical constants of water in the 200-nm to 200- μ m wavelength region. *Appl. Opt.*, **12**, 555-563.
- Hasted, J. B., 1973: *Aqueous Dielectrics*. Halsted Press, 302 pp.
- Hobbs, P. V., 1974: *Ice Physics*. Oxford Press, 837 pp.
- Jameson, A. R., 1991: A comparison of microwave techniques for measuring rainfall. *J. Appl. Meteor.*, **30**, 32-54.
- Jameson, A. R., 1992: The effect of temperature on attenuation-correction schemes in rain using polarization propagation differential phase shift. *J. Appl. Met.*, **31**, 1106-1118.
- Johari, G. P., 1976: The dielectric properties of H₂O and D₂O ice Ih at MHz frequencies. *J. Chem. Phys.*, **64**, 3998-4005.
- Johari, G. P., 1981: The Spectrum of Ice. *Contemp. Phys.*, **22**, 613-642.
- Kopelevich, O. V., 1976: Optical properties of pure water in the 250-600 nm range. *Opt. Spektrosk.*, **41**, 391-392.
- Kou, L., D. Labrie, and P. Chylek, 1993: Refractive indices of water and ice in the 0.65- to 2.5- μ m spectral range. *Appl. Opt.*, **32**, 3531-3540.
- Lawson, C. L., and R. J. Hanson, 1974: *Solving Least Squares Problems*. Prentice-Hall, 340 pp.
- Liu, G., and J. A. Curry, 1992: Retrieval of precipitation from satellite microwave measurement using both emission and scattering. *J. Geophys. Res.*, **97**, 9959-9974.
- Malmberg, C. G., and A. A. Maryott, 1956: Dielectric constant of water from 0° to 100° C. *J. Res. Nat. Bur. Stand.*, **56**, 1-8

- Palmer, K. F., and D. Williams, 1974: Optical properties of water in the near infrared. *J. Opt. Soc. Am.*, **64**, 1107-1110.
- Pinkley, L. W., P. P. Sethna, and D. Williams, 1976: Optical constants of water in the infrared: Influence of temperature. *J. Opt. Soc. Am.*, **67**, 494-499.
- Pounder, E. R., 1965: *The Physics of Ice*. Pergamon Press Ltd., 151 pp.
- Ray, P. S., 1972: Broadband complex refractive indices of ice and water. *Appl. Opt.*, **11**, 1836-1844.
- Robertson, C. W., B. Curnutte, and D. Williams, 1973: The infrared spectrum of water. *Mol. Phys.*, **26**, 183-191.
- Sadiku, M. N. O., 1985: Refractive index of snow at microwave frequencies. *Appl. Opt.*, **24**, 572-575.
- Schaaf, J. W., and D. Williams, 1973: Optical constants of ice in the infrared. *J. Opt. Soc. Am.*, **63**, 726-732.
- Schwan, H. P., R. J. Sheppard, and E. H. Grant, 1976: Complex permittivity of water at 25 °C., *J. Chem. Phys.*, **64**, 2257-2258.
- Sheppard, R. J., 1973: The least-squares analysis of complex weighted data with dielectric applications. *J. Phys. D: Appl. Phys.*, **6**, 790-794.
- Shimabukuro, F. I., M. T. Tavis, and D. S. Chang, 1984: EHF attenuation derived from emission temperatures in light rain. *Radio Sci.*, **19**, 1535-1542.
- Srinivasan, K. R. and R. L. Kay, 1974: Pressure dependence of the dielectric constant of H₂O and D₂O. *J. Chem. Phys.*, **60**, 3645-3649.
- Warren, S. G., 1984: Optical constants of ice from the ultraviolet to the microwave. *Appl. Opt.*, **23**, 1206-1224.
- Wooten, F., 1972: *Optical Properties of Solids*. Academic Press, 260 pp.
- Wörz, O., and R. H. Cole, 1969: Dielectric properties of ice I. *J. Chem. Phys.*, **51**, 1546-1551.

Zoloratev, V. M., and A. V. Demin, 1977: Optical constants of water over a broad range of wavelengths, 0.1 Å-1 m. *Opt. Spektrosk.*, **43**, 157-161.

BIOGRAPHICAL SKETCH

Mark Lee Mesenbrink [REDACTED]

[REDACTED] He entered the University of Oklahoma on a 4 year Air Force Reserve Officer Training Corps scholarship and received a Bachelors of Science with distinction in Electrical Engineering in the summer of 1990. He was commissioned as a Second Lieutenant in the Air Force on 6 August, 1990. After being activated on 5 June, 1991, he entered the Basic Meteorology Program at the University of Oklahoma where he was awarded a Bachelors of Science in Meteorology in the Spring of 1992. After a 2 year tour of duty at Dyess Air Force Base near Abilene, Texas, as an operational forecaster and staff meteorologist, he entered the Air Force Institute of Technology civilian institution program at Florida State University where he pursued a Masters of Science in Meteorology.